Bulk-cone singularities & signatures of horizon formation in AdS/CFT

Veronika E Hubeny,[a] **Hong Liu**[b] **and Mukund Rangamani**[a]

[a] *Centre for Particle Theory & Department of Mathematical Sciences*
Science Laboratories
South Road, Durham DH1 3LE, United Kingdom
[b] *Center for Theoretical Physics , Massachusetts Institute of Technology*
Cambridge, Massachusetts, 02139, U.S.A.
E-mail: `veronika.hubeny@durham.ac.uk`, `hong_liu@lns.mit.edu`,
`mukund.rangamani@durham.ac.uk`

ABSTRACT: We discuss the relation between singularities of correlation functions and causal properties of the bulk spacetime in the context of the AdS/CFT correspondence. In particular, we argue that the boundary field theory correlation functions are singular when the insertion points are connected causally by a bulk null geodesic. This implies the existence of "bulk-cone singularities" in boundary theory correlation functions which lie inside the boundary light-cone. We exhibit the pattern of singularities in various asymptotically AdS spacetimes and argue that this pattern can be used to probe the bulk geometry. We apply this correspondence to the specific case of shell collapse in AdS/CFT and indicate a sharp feature in the boundary observables corresponding to black hole event horizon formation.

KEYWORDS: AdS-CFT Correspondence, Black Holes in String Theory.

Contents

1. Introduction

The AdS/CFT correspondence, which relates quantum gravity in asymptotically Anti de Sitter spacetimes to a non-gravitational gauge theory, is an invaluable window to understanding effects of gravity beyond the semi-classical approximation. In principle the correspondence provides a framework to address many long standing questions in quantum gravity, such as the nature of singularity resolution or issues relating to the information paradox. While much has been learnt in the past few years, the status of the dictionary between gravitational quantities and field theory observables is still at a somewhat rudimentary stage. This has been a stumbling block for exploiting the correspondence to its full power, especially in eliciting answers to oft posed quantum gravitational questions.

In classical general relativity, concepts such as causal structure, event horizons, singularities, *etc.*, play an important role in understanding the geometry of the spacetime manifold. In the semi-classical approximation these concepts are useful in understanding the dynamics of quantum fields in curved backgrounds. Given the AdS/CFT correspondence it is interesting to understand field theoretic encoding of these geometric concepts. Considering the central role played by geometry in classical general relativity, one naively expects them to have a well defined representation in the field theory.

For instance, consider the field theoretic representation of bulk causal structure. In the semi-classical limit, the bulk causal structure can be read off from the properties of correlation functions of quantum fields propagating on the spacetime manifold. For asymptotically AdS spacetimes the bulk correlation functions in turn determine (in some suitable scaling limit) the boundary correlation functions. Consistency within the correspondence requires therefore that the boundary correlation functions are compatible with the bulk causality constraints. This has been demonstrated to be true in many examples [1–4]. A crucial ingredient in most of these analyses has been to exploit the asymptotic AdS geometry where consistency is guaranteed by the symmetries in question.

The non-trivial aspect of the geometry that one would like to understand is the behaviour of the bulk causal structure deep in the interior of an asymptotically AdS spacetime. For example one can ask whether the presence of an event horizon in the spacetime has a non-trivial signature in the boundary. The zeroth order answer to this question, at least for eternal black holes in AdS spacetime, is that the dual field theory is in a thermal state.[1] So the presence of the horizon is encoded in a new scale for physics in the boundary theory, the thermal scale. However, this information hardly probes the causal structure in the vicinity of the horizon.

---

[1]This is true only for black holes whose horizon size is larger than the AdS scale.

Furthermore, since the AdS/CFT correspondence is most firmly understood in the Euclidean framework, questions pertaining to genuinely time-dependent processes in the bulk and holographic duals thereof become much more subtle. For example, consider modelling a time dependent process, such as of black hole formation in the bulk, within the field theory. A more nuanced question, then, would to ask whether there is any field theory information to be gained about the event horizon formation process. Phrased differently: *can we see horizon formation directly in the gauge theory?* Since in the bulk the event horizon forms at a sharply-localized event[2] (despite the fact that we need to know the full future evolution of the spacetime to actually find the horizon), we would expect that this will manifest itself in some correspondingly sharp feature in the gauge theory.

The conventional lore is that the UV/IR relation, which maps local regions in the interior of the bulk to non-local objects in the CFT, makes it hard to extract useful information about bulk geometry (*cf.*, [5] for attempts to use UV/IR relation to extract information about the horizon). Given that the geometric scale associated with the horizon corresponds to the thermal scale for neutral black holes, it is hard to see how to extract a precise signal about the causal structure in the neighbourhood of the event horizon.

The clue comes from the progress made in the recent past in identifying the CFT signature of the black hole singularity [6, 7]. In this case the field theoretic observables transcend the classical barrier of the event horizon to encode information of behind the horizon physics. The main observation of [6], which built on the original work of [8, 9] was to use the intrinsic non-locality of the boundary correlation functions to identify signals of the singularity. The black hole singularity was identified to correspond to a particular 'light-cone' like singularity in the field theory correlation function.[3] It has further been proposed that this technique can be exploited to understand physics behind the event horizon and in particular used to investigate aspects of inflationary geometry within AdS/CFT [10]. The basic idea was to look at the bulk Green's functions in a saddle approximation where they are dominated by geodesics and use the bulk computations to derive predictions for boundary correlation functions.

In the present work we argue that the horizon formation in gravitational collapse can be detected in the boundary theory by examining the structure of singularities of generic Lorentzian correlators. In particular, we show that a sharp horizon-formation time can be extracted from the pattern of singularities.

Our argument is based on a connection between null geodesics in the bulk spacetime and singularities in correlation functions of local operators evaluated in the state corresponding to the bulk geometry.[4] The basic idea is that CFT correlators will exhibit light-cone singularities when the points of operator insertion are connected by a null geodesic.

---

[2]In this work we consider spherically symmetric spacetimes. More generally, in non-spherical spacetimes the event horizon could form at a locus of events; our methods should generalise to these cases as well.

[3]The identification of the singularity in the strict large N limit is easiest when formulated in terms of momentum space correlators [7] as opposed to direct computation in position space where the singularity is not visible in the primary sheet of the correlator [6]. In particular, it was confirmed in [7] that the signatures of the singularities go away when the rank of the boundary theory gauge group is finite, implying that the singularities are resolved in quantum gravity.

[4]Spacetimes which are asymptotically AdS can be thought of as deformations of pure AdS by normaliz-

The connection implies that CFT correlators in excited states have additional Lorentzian singularities inside the light cone, which we will call *bulk-cone singularities*. Usually CFT correlators exhibit light-cone singularities and the location of these is determined by the causal structure of the background spacetime on which the field theory lives. For a CFT living on $\mathbf{R} \times \mathbf{S}^{d-1}$ these would be given by the conventional light cone of the Einstein static universe. Our main observation is that bulk causality, together with the dictionary between bulk Green's functions and boundary correlation functions in the AdS/CFT context, necessitates additional bulk-cone singularities in the CFT correlators.

Armed with this relation we can ask how certain geometric structures are encoded in the boundary data. In addition to a black hole collapse geometry which motivated this study, we also look at the geometry of a star in AdS spacetime and the eternal black hole geometry. In all these cases, interesting details about the geometry and its causal structure that can be read off from the properties of the singularities in the CFT correlators. In fact, as has recently been shown in [11], the location of the boundary singularities can be used to reconstruct the complete bulk metric for a class of static, spherically symmetric spacetimes. Our analysis is carried out by explicitly studying geodesics in the bulk spacetime and using this to infer properties about correlation functions in strongly coupled gauge theories. While there are a few consistency checks we can establish in some simple cases, many of our results are predictions for strong coupling CFT correlation functions in certain excited states.

The plan of the paper is as follows: We begin in section 2 by motivating our claim that Lorentzian AdS/CFT correspondence implies that correlation functions of local operators evaluated in excited states of the field theory exhibit light-cone singularities whenever the operator insertion points are connected by null geodesics through the bulk spacetime. We then confirm the relation between light-cone singularities and bulk null geodesics for vacuum correlators. Further, we generalize to excitations about vacuum state and obtain predictions for the singularities in the correlation functions from the behaviour of null geodesics. To demonstrate how sensitively the singularity pattern depends on the state, in Sections 3 and 4 we explicitly study the nature of the singularities and their implications for correlation functions in two scenarios: a generic excited state and a thermal state, which we model in the bulk by a star in AdS and an eternal black hole geometry, respectively. We devote section 5 to our main example, the collapse of a black hole in AdS spacetime, and elicit from the geometry signatures of event horizon formation in the field theory. We conclude in section 6 with a discussion. Finally, in the Appendices we present more detailed calculations pertaining to the various geometries considered (pure AdS, star in AdS, eternal Schwarzschild-AdS, Poincare patch, null shell collapse, and Vaidya-AdS).

2. Null geodesics and boundary singularities

In this section we motivate a simple relation between singularities of the boundary correlation functions and null geodesics in the bulk spacetime. The main idea is to exploit the

---

able modes in the supergravity description. In field theory terms this corresponds to a generic excited state obtained by acting on the CFT vacuum with the appropriate operator.

AdS/CFT dictionary for evaluating strong coupling correlation functions in the CFT using bulk Green's functions. Since the bulk Green's functions are sensitive to the bulk causal structure we expect that the properties of the bulk light cone to be directly visible in the boundary correlation functions.

A short word on notation: for convenience, we will denote the $d + 1$ dimensional bulk spacetime by $\mathcal{M}$ and its d dimensional boundary by $\partial \mathcal{M}$. Further, we use labels x, y *etc.*, for points on the boundary $\partial \mathcal{M}$ and r to denote the radial coordinate normal to $\partial \mathcal{M}$.

2.1 General argument

The AdS/CFT correpsondence gives us a precise map relating string theory (or its low energy supergravity limit) on $\mathcal{M}$ with a field theory living on the boundary $\partial \mathcal{M}$ of $\mathcal{M}$. To be precise, in the low energy supergravity approximation of the bulk theory (which is good as long as we choose the 't Hooft coupling λ and the rank of the gauge group N on the boundary to be large, *i.e.*, $\lambda \gg 1$ and $N \gg 1$) we can obtain the boundary correlation function $G(x, x')$ from the bulk propagator $\mathcal{G}(x, r; x'; r')$ of the corresponding field by taking both end points to the boundary. More precisely,

$$G(x, x') = 2 \nu \lim_{r \to \infty, r' \to \infty} (rr')^\Delta \, \mathcal{G}(x, r; x'; r') \ , \tag{2.1}$$

where $\mathcal{G}$ is the free field theory propagator for the corresponding bulk field. Focussing on the simple case of local gauge invariant operators $\mathcal{O}(x)$ of conformal dimension Δ in $\partial \mathcal{M}$ which are dual to free scalar fields parameterized by mass m in the bulk, in (2.1) we have

$$\Delta = \frac{d}{2} + \nu \ , \qquad \nu = \sqrt{m^2 + \frac{d^2}{4}} \ , \tag{2.2}$$

where we have set the curvature radius of AdS to be 1. Note that by choosing the asymptotic AdS time to coincide with the boundary time, one ensures that time ordering chosen for the bulk propagator $\mathcal{G}$ carries over to the boundary correlator in the limiting procedure. In what follows we will consider Feynmann propagators.

That the limit in (2.1) is well-defined for an asymptotically AdS spacetime can be seen as follows. Upon fixing (x', r'), $\mathcal{G}(x, r; x', r')$ is a normalizable solution of the free bulk wave equation on $\mathcal{M}$. This implies for an asymptotically AdS spacetime

$$\mathcal{G}(x, r; x', r') \sim r^{-\Delta}, \qquad r \to \infty \ . \tag{2.3}$$

Similarly,

$$\mathcal{G}(x, r; x', r') \sim r'^{-\Delta}, \qquad r' \to \infty \ . \tag{2.4}$$

Thus for generic boundary points x and x', the limit (2.1) is well defined and yields a regular $G(x, x')$. However, if x and x' are connected by a null geodesic, (2.3) and (2.4) could break down, in which case one expects

$$\lim_{r, r' \to \infty} \mathcal{G}(x, r; x'; r') \not\to 0 \ . \tag{2.5}$$

A naive application of (2.1) will yield a divergent answer as the limit is not well-defined.

In order to obtain explicitly the singular behavior of $G(x, x')$ has to work with a suitably regularized expression. To this end one can first consider some x'' lying in a small neighborhood of x' in the boundary. If x'' is not connected to x by null geodesics, (2.1) can be straightforwardly applied to obtain $G(x, x'')$. One can then take $x'' \to x'$ to obtain the desired correlator $G(x, x')$.

We will now motivate the above discussion in a slightly different perspective using the geodesic approximation to $\mathcal{G}(x, r; x', r')$. For this purpose, we will take m large[5] so that $\Delta \approx m$. To consider the limit (2.1), we put the boundary $\partial \mathcal{M}$ at a cut-off surface $r = r' = \Lambda \to \infty$, on which (for an asymptotically AdS geometry) the induced metric can be approximated as

$$ds^2 = \Lambda^2 \, ds_{bd}^2 \tag{2.6}$$

where ds_{bd}^2 denotes the metric on the boundary $\partial \mathcal{M}$.

Consider points $A = (x, \Lambda)$ and $B = (x', \Lambda)$ on the cut-off surface, which are spacelike separated. In the large m limit, one expects that the saddle point approximation is valid. Denoting by $d(A, B)$ the proper distance between two (spacelike separated) points in $\mathcal{M}$ we have

$$\mathcal{G}(A, B) \propto e^{-m \, d(A,B)} \sim e^{-2m \log \Lambda} \ , \tag{2.7}$$

where we used the fact that as $\Lambda \to \infty$, the proper distance $d(A, B) \approx 2 \log \Lambda + \cdots$ in asymptotically AdS spacetimes. Note that (2.7) is consistent with (2.3) and (2.4) and hence makes sure that the limit (2.1) is well defined.[6]

Now suppose that there is a null geodesic connecting A and B – in this case $d(A, B) = 0$ and $\mathcal{G}(A, B) \sim O(1)$. As suggested above we consider points $C = (x'', \Lambda)$ in a small neighborhood of B, for which

$$d(A, C) \sim \log[\Lambda^2 \, \delta x^2] \tag{2.8}$$

where δx is the proper distance between x and x'' on the boundary (i.e., in terms of metric ds_{bd}^2 in (2.6) on $\partial \mathcal{M}$). Plugging (2.8) into (2.7) and then taking the limit as suggested in (2.1), we have

$$G(x, x'') \sim \frac{2m}{(\delta x^2)^m}, \qquad x'' \to x' \ . \tag{2.9}$$

To summarize, we have argued that a boundary correlation function $G(x, x') = \langle \mathcal{O}(x) \mathcal{O}(x') \rangle$ is singular if and only if [7] there exist null geodesics connecting x and x'. Our argument is not completely rigorous and we discuss potential loopholes below. This proposal can be checked in simple examples in which one can work out the boundary $G(x, x')$ explicitly, like global pure AdS, Poincare patch and the BTZ black holes (see appendices).

---

[5]The relation between null geodesics and singularities of $G(x, x')$ does not require taking m large.

[6]For generic timelike separated points A, B on $\partial \mathcal{M}$, we also expect (2.7) to be true based on analytic continuation from spacelike separated points. Note that in the pure AdS, $\mathcal{G}$ is a function of the proper distance $d(A, B)$ which can be analytically continued in the complex plane to timelike separation.

[7]While we have explicitly shown that bulk null geodesics lead to new singularities in boundary correlation functions, our arguments indicate that the converse should also be true. This is equivalent to the statement that (2.5) is true only for points connected by null geodesics.

2.2 Types of null geodesics and causal structure

In this subsection we discuss the location of the singularities in $G(x, x')$ and structure of null geodesics. For this purpose, let us fix x and consider those x' which are connected to x by null geodesics. The null geodesics can be divided into two types: those lying entirely in the boundary (type $\mathcal{A}$) and those lying in the bulk except for their end points (type $\mathcal{B}$). Type $\mathcal{A}$ geodesics are simply null geodesics of the boundary theory and define the light cone of the CFT. For points x and x' connected by Type $\mathcal{A}$ null geodesics, $G(x, x')$ has the standard light-cone singularities. Type $\mathcal{B}$ null geodesics are more interesting and we now discuss them in some detail.

In pure global AdS (where the boundary is $\mathbf{R} \times \mathbf{S}^{d-1}$), all Type $\mathcal{B}$ null geodesics connect the anti-podal points on S^{d-1}. The points in question are given by (t_i, Ω) and $(t_o, -\Omega)$, with $t_o - t_i = \pi R_{AdS} = \pi$ and $\pm\Omega$ denote points which are anti-podal on the $\mathbf{S}^{d-1}$. Note that the (boundary) time separation $t_o - t_i = \pi$ needed for the geodesic to traverse the bulk is exactly the same as that of a Type $\mathcal{A}$ null geodesic connecting the anti-podal points only in pure AdS spacetime; the former becomes longer for general asymptotically AdS spacetimes. Further details on geodesics in AdS, both analytic and pictorial, appear in appendix A.

Since in the case of pure AdS the end points of the Type $\mathcal{B}$ null geodesics already coincide with the boundary light cone, they do not give rise to additional singularities in the boundary correlation functions. It is easy to verify that the behaviour of null geodesics in AdS is consistent with the singularity properties of boundary correlation functions. The boundary correlators in questions are two-point functions in the CFT vacuum of primary operators of dimension Δ which for a d-dimensional CFT on $\mathbf{R} \times \mathbf{S}^{d-1}$ are given by

$$\langle \mathcal{O}(t, \Omega) \, \mathcal{O}(t', \Omega') \rangle \propto \frac{1}{(\cos(t - t') - \cos(\Omega - \Omega'))^{\Delta}} \, , \qquad (2.10)$$

The singularities of the correlation function (2.10) are given by $\delta t = \delta\Omega$ with $\delta t = t - t'$, *etc.*, which coincide with the light cone of the boundary manifold.

In a perturbed AdS spacetime, the end points of Type $\mathcal{B}$ geodesics in general do not coincide with the light cone of the boundary manifold. They will therefore give rise to additional singularities in the boundary correlation functions. We will call such singularities *bulk-cone singularities*. An interesting feature of asymptotically AdS spacetimes is that there exists a lower bound on the 'time delay' experienced by geodesics exploring the bulk spacetime. In a situation where the bulk manifold $\mathcal{M}$ with a timelike conformal boundary $\partial\mathcal{M}$ satisfies the null energy condition, the null generic condition, and strong causality and compactness, it has been proven by Gao and Wald [3] that the end points x' of Type $\mathcal{B}$ geodesics always lie *inside* the light cone of the boundary manifold, *i.e.*, x' and x are timelike separated. This implies that any generic perturbation of AdS (satisfying the conditions mentioned) will produce a time delay of null geodesics relative to pure AdS. For example, imagine a state corresponding to a thermal gas in AdS at some internal mass density ρ_o. Then a radial geodesic will arrive to the anti-podal point of the boundary after a time Δt which increases monotonically with increasing ρ_o.

This implies that correlation functions in some excited states[8] of the theory will have additional Lorentzian singularities inside the light cone. We also note that it can be checked explicitly that for backgrounds with non-compact boundary, Type $\mathcal{B}$ null geodesics do not exist for states preserving the boundary symmetries (for a proof of the statement see appendix D). Thus additional singularities appear to arise only for CFTs on compact spaces or those that violate the Poincaré symmetery for CFT on $\mathbf{R}^{3,1}$.

While the theorem of Gao and Wald only applies to asymptotically AdS spacetime satisfying the conditions stated above, from the causality of the boundary theory one would like to conclude that the end points of Type $\mathcal{B}$ null geodesics should always lie inside the light cone of the boundary for any asymptotically AdS background with a field theory dual. Otherwise it would imply that one can set up a special state in the field theory to transmit signals faster than the speed of light (see also [12]).

To conclude this section let us comment on a potential loophole in our argument. Our connection between null geodesics and singularities of boundary correlation functions is based on the validity of (2.5) for any two points connected by a null geodesic. While this assumption is consistent with our general understanding of quantum field theory in a curved spacetime, we do not have a rigorous proof of the statement.[9] Also note that one should distinguish between points which can be connected by a null geodesic and those points which the geodesics connecting them only *approach* null. In the latter case, when there does *not* exist a null geodesic which connects two points, our argument does not directly apply. We will elaborate more on this when discussing the gravitational collapse background in section 5.

3. Static asymptotically AdS geometries

We now turn to applying the results of section 2 to static spacetimes. A trivial example where our relations can be verified is of course the empty AdS spacetime which we have already commented on. We now turn to consider geometries which are deformations of AdS, with a free parameter such that pure AdS is retrieved in a particular limit of this parameter. We will first consider situations with sufficient symmetries to simplify the analysis before turning to more complicated examples. For concreteness, we will work in 5

---

[8]In order to have non-negligible back reaction on the bulk metric, the ADM mass M of the perturbation should satisfy $G_N M \sim \mathcal{O}(1)$. This implies that the corresponding excited state in boundary theory should have energy of order $\mathcal{O}(N^2)$. In the following discussion, by generic excited states, we mean generic states of such energies.

[9]For example, in a semi-classical approximation to the propagator, one may consider the following scenario: In general, the end points of a null geodesics can be shared by other spacelike and/or timelike geodesics. If the propagator is given by summing over all geodesics, then the null geodesic clearly dominates. However, there might be a situation that path integration contours for the propagator cannot be deformed to the saddle point corresponding to the null geodesic. Then the null geodesic will not contribute to the propagator, even though it naively dominates. Analogous phenomenon was encountered in [6] for a spacelike (almost null) geodesic 'bouncing off' a black hole singularity; though it is not clear whether this contingency will ever arise for strictly null geodesics. Given that one can send light signals following null geodesics, one might be able to argue a null geodesic should always contribute to a propagator.

dimensions, *i.e.*, take the spacetime to be asymptotically AdS_5 (times a $\mathbf{S}^5$ which will not play any role).

3.1 Geometries of stars in AdS

As our first nontrivial example, we will take our spacetime to be static and spherically symmetric, and to make things even simpler, we will take the matter content to be that of a self-gravitating gas of radiation. We note that self-gravitating radiation in AdS has been explored previously in [13] and related geometries of boson stars in asymptotically AdS spacetimes have been considered in *e.g.* [14, 15]. The symmetries imply the corresponding stress tensor is that of a perfect fluid; radiation equation of state which makes the stress tensor traceless, *i.e.*,

$$T_{ab} = \rho(r)\, u_a\, u_b + P(r)\, (g_{ab} + u_a\, u_b)\,, \qquad P = \frac{1}{4}\, \rho \tag{3.1}$$

where u^a is a co-moving gas 4-velocity, and $\rho(r)$, $P(r)$ are density and pressure. Since the radiation will be confined by the AdS potential, we will refer to this configuration as a "star" in AdS. The metric can be obtained by solving the Einstein's equations with negative comological constant and the requisite stress tensor, as discussed in detail in appendix B. Here we summarize the main results.

The metric can be written in the form:

$$ds^2 = -f(r)\, dt^2 + h(r)\, dr^2 + r^2\, d\Omega_3^2 \tag{3.2}$$

with

$$h(r) = \left[r^2 + 1 - \frac{m(r)}{r^2} \right]^{-1} \tag{3.3}$$

and

$$f(r) = \left(\frac{\rho_\infty}{\rho(r)} \right)^{2/5} \tag{3.4}$$

where the mass function $m(r)$ is defined in terms of an integral of the density $\rho(r)$,

$$m(r) \equiv \frac{2}{3} \int_0^r \rho(\bar{r})\, \bar{r}^3\, d\bar{r} \tag{3.5}$$

and ρ_∞ is the coefficient of the leading fall-off of $\rho(r)$, determined by $\rho(r) \sim \rho_\infty/r^5$ as $r \to \infty$. The field equations specify the system of coupled first order ODEs which $m(r)$ and $\rho(r)$ must satisfy:

$$m'(r) = \frac{2}{3}\, \rho(r)\, r^3 \tag{3.6}$$

$$\rho'(r) = -5\, \frac{\rho(r)}{r} \left(\frac{r^2 + \frac{m(r)}{r^2} + \frac{1}{12}\, \rho(r)\, r^2}{r^2 + 1 - \frac{m(r)}{r^2}} \right) \tag{3.7}$$

with boundary conditions $m(0) = 0$ and $\rho(0) \equiv \rho_0$, where ρ_0 is a free parameter of the configuration, specifying the internal density of the gas. Thus the geometries are parameterized by a single parameter ρ_0, with pure AdS retrieved in the $\rho_0 = 0$ case.
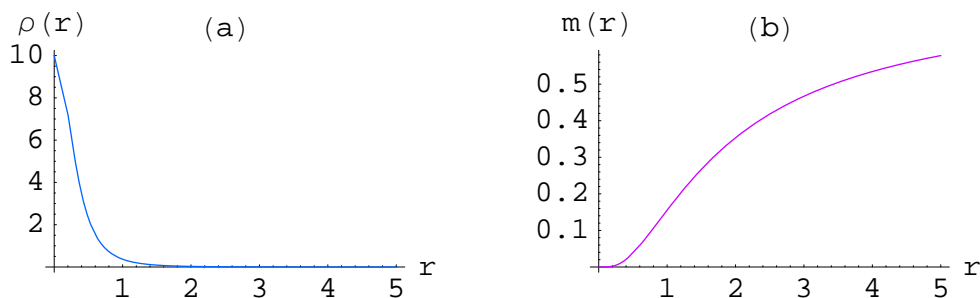
Figure 1: Density and mass functions for the "star" geometry, where the central density is set to $\rho_0 = 10$.
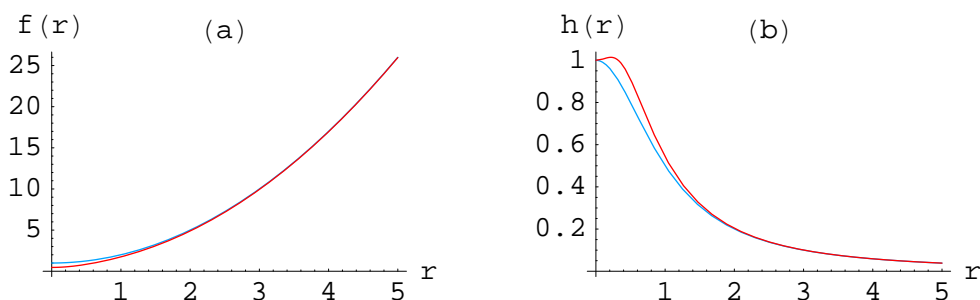

Figure 2: Metric functions for the "star" geometry with central density $\rho_0 = 10$ (red curves), and for comparison corresponding metric functions in the pure AdS geometry (blue curves; $f(r)$ is the higher and $h(r)$ is the lower of the two curves).

From (3.6) and (3.7) we find the following asymptotic behavior for $m(r)$ and $\rho(r)$

$$r \to \infty: \qquad \rho(r) \to \frac{\rho_\infty}{r^5}\left(1 - \frac{5}{2r^2} + \frac{5(4M+7)}{8r^4} + \cdots\right), \tag{3.8}$$

$$m(r) \to M - \frac{\rho_\infty}{r} + \cdots \tag{3.9}$$

$$r \to 0: \qquad \rho(r) \to \rho_0 + O(r^2), \qquad m(r) \to \frac{\rho_0}{6}r^4 + O(r^6) \tag{3.10}$$

where ρ_∞ and M (M is proportional to ADM mass) are constants which are determined by ρ_0. Using (3.3) and (3.4) we also find that

$$r \to \infty: \qquad f(r) \to r^2 + 1 - \frac{M}{r^2} + \cdots \qquad h(r) \to \left[r^2 + 1 - \frac{M}{r^2} + \cdots\right]^{-1} \tag{3.11}$$

$$r \to 0: \qquad f(r) \to \left(\frac{\rho_\infty}{\rho_0}\right)^{\frac{2}{5}} + O(r^2), \qquad h(r) \to 1 + O(r^2) \tag{3.12}$$

One can readily solve the full equations (3.6) and (3.7) numerically. Figure 1 shows the density and mass functions for the internal density $\rho_0 = 10$.

The metric functions are plotted in figure 2, again for the same set-up as in figure 1. For comparison we also plot the corresponding metric coefficients for pure AdS; as we would expect, the metric does approach that of AdS as the density becomes small.
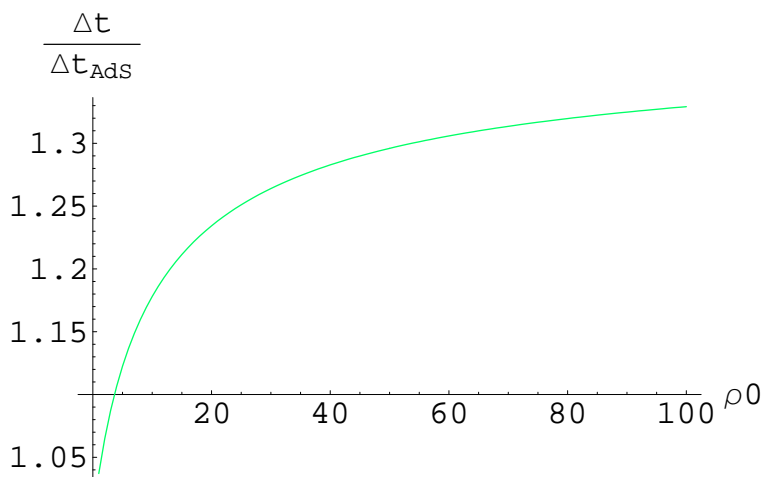
Figure 3: Time delay for radial null geodesics through star in AdS, as a function of the star's internal density ρ_0.

3.2 Geodesics in the star AdS geometry

We will now turn to the properties of bulk null geodesics (Type $\mathcal{B}$) in the star geometry. Staticity and spherical symmetry implies that E (energy) and J (angular momentum) are conserved along any geodesic and hence we will parameterize the geodesics by these quantities. The equations for null geodesics are:

$$\dot{t} = \frac{\alpha}{f(r)} \,, \qquad \dot{\varphi} = \frac{1}{r^2} \,, \qquad \text{and} \qquad f(r)\, h(r)\, \dot{r}^2 = \alpha^2 - V(r) \,, \tag{3.13}$$

where

$$V(r) = \frac{f(r)}{r^2}, \qquad \alpha \equiv \frac{E}{J} \tag{3.14}$$

and the dot denotes differentiation with respect to the affine parameter along the geodesic. For null geodesics the absence of scale implies that the relevant parameter is the ratio $\alpha = E/J$. Useful quantifiers for figuring out which points on the boundary are connected by null geodesics are the temporal and angular separation of the geodesic endpoints, which we denote by Δt and $\Delta \varphi$, respectively. Since we have a numerical solution for the metric, we have to integrate the geodesic equations numerically to find the desired properties.

Consider first radial null geodesics, which we expect will emerge at a later time than the corresponding geodesic in pure AdS, consistent with the theorem of [3]. Denoting this time by Δt_0, we have

$$\Delta t_0 = 2 \int_0^\infty \sqrt{\frac{h(r)}{f(r)}} \, dr \tag{3.15}$$

For a star geometry with central density $\rho_0 = 10$, we find numerically that $\Delta t_0 \approx 3.696$, which is 1.177 times longer than in pure AdS. Figure 3 exhibits the dependence of this time delay on the value of ρ_0. We see that while the time delay increases monotonically with increasing density, it does so more and more slowly.[10]

---

[10]The intuitive reason for Δt_0 not increasing more rapidly with ρ_0 is that the larger the internal density
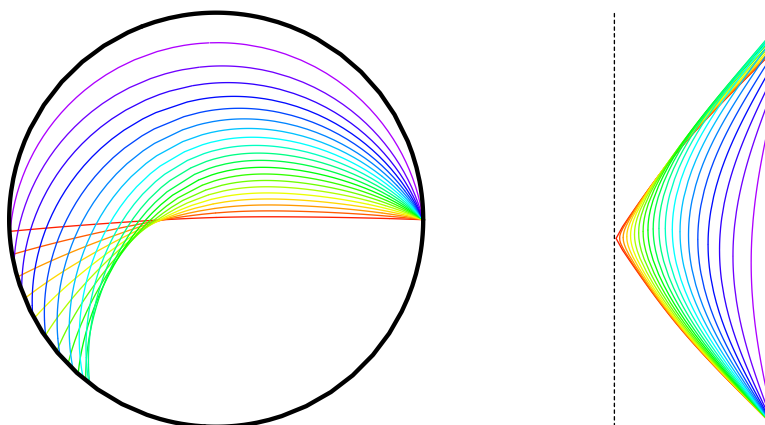
Figure 4: Null geodesics in star with $\rho_0 = 10$ in AdS, projected onto a constant t slice and the $t - r$ plane, for varying angular momentum to energy ratio ($E = 10$ and $J = 0, 1, \ldots, 10$). On the left, the bold circle corresponds to the AdS boundary, whereas on the right, the dashed vertical line corresponds to the origin $r = 0$ and the bold vertical line to the boundary at $\tan r = \frac{\pi}{2}$. The range of t plotted is $(0, 1.1 \, \Delta t_0)$. (Analogous plots with larger ρ_0 appear in figure 19 of appendix B.)

Now let us consider null geodesics with nonzero angular momentum. (Appendix B further explores non-radial spacelike geodesics.) In figure 4, we show null geodesics projected onto a spatial (constant t) slice (left) and the $t - r$ plane (right). Not surprisingly, the star has a focusing effect on the geodesics. The important point to note is that now, unlike the pure AdS case, there is a finite spread of the Δt and $\Delta \varphi$ endpoint values the null geodesics can take. More specifically, because of the attractive nature of the star's gravitational potential, the small angular momentum ($J/E \ll 1$) geodesics 'overshoot' in terms of angular separation, and at the same time they experience some time delay, which means that both Δt and $\Delta \varphi$ increase. However, this effect does not keep increasing monotonically with increasing angular momentum, because the further from the origin the geodesics penetrate, the less effect of the star they feel. In the high angular momentum limit ($J/E \sim 1$), the geodesics hug the boundary and consequently behave just as the corresponding geodesics in pure AdS.

To illustrate explicitly how the endpoints of these various geodesics compare, figure 5 summarizes the behaviour of Δt and $\Delta \varphi$ for the various geodesics. In (a), where the endpoints are plotted for small internal densities, $\rho_0 = 1, \ldots, 10$, we see that the effect of overshooting becomes more pronounced the higher ρ_0 is. In (b), where $\rho_0 = 10, \ldots, 100$, we illustrate that the effect however remains bounded even for high internal densities. (We have verified this numerically for $\rho_0 \lesssim 10^{18}$.) Note that the Δt intercept for each curve can be read off already from figure 3.

The boundedness of Δt implies one of the interesting features for the star geometries, namely the absence of null geodesics orbiting the star. In fact, one can obtain this result

---

ρ_0, the faster the density function $\rho(r)$ falls off, in such a way as to keep the total mass M bounded, as discussed in appendix B. Numerically we find that Δt_0 appears to be bounded as $\rho_0 \to \infty$.
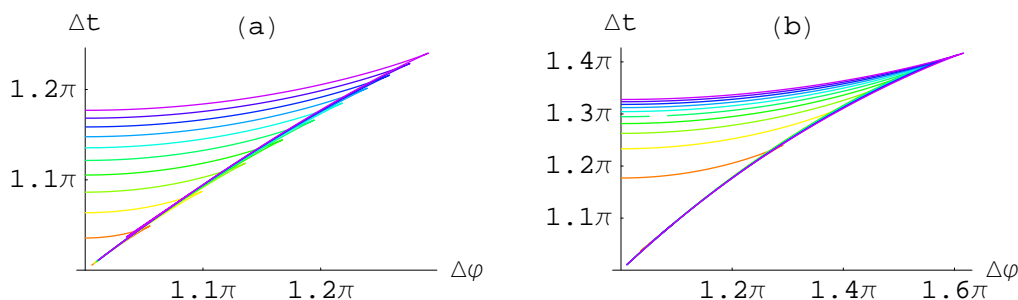
Figure 5: Endpoints of null geodesics in the AdS geometry of star with **(a)** $\rho_0 = 1, 2, \ldots, 10$ and **(b)** $\rho_0 = 10, 20, \ldots, 100$. Each curve is plotted by varying $\alpha = \frac{E}{J}$. The top of the curves corresponds to big values of α; in fact, one can easily show that the slope of each curve (as a function of α) is given by $1/\alpha$.

more directly, as follows: From (3.13) we see that in order to have null geodesics at fixed radial distance from the star, *i.e.*, $r(\lambda) = $ constant, we require that $\alpha^2 - V(r) = 0$ and $\frac{d}{dr}V(r) = 0$. It is easy to show numerically that these conditions are never satisfied for the star geometries.[11] As we will argue below, this absence of circular orbits around the star leads to marked differences in the behaviour of singularities for correlation functions in the pure state corresponding to the star and in themal density matrix represented by an eternal black hole geometry. In particular, in the star case, the spread of the geodesic endpoints remains bounded, unlike for the black hole case which has a circular orbit.

The essential points relating to null geodesics in the star background can be summarized as follows:

- The radial null geodesics which go through the bulk geometry emerge at the antipodal point on the sphere ($\Delta\varphi = \pi$) at a later time than in pure AdS ($\Delta t > \pi$). The time delay is a monotonic function of the internal density ρ_0.

- Null geodesics with angular momentum exhibit both a time delay as well as a shift in $\Delta\varphi$. For small angular momentum, both Δt and $\Delta\varphi$ increase with increasing angular momentum, whereas for large angular momentum they decrease to match with the AdS value $\Delta t = \Delta\varphi = \pi$ when $J = E$. While this effect increases with increasing ρ_0, Δt and $\Delta\varphi$ remain bounded for arbitrary ρ_0.

- There are no null geodesics at fixed value of the radial coordinate *i.e.*, the star spacetime does not admit circular photon orbits.

We stress that since the endpoints of the null geodesics indicate the location of a singularity in the corresponding correlation function as discussed above, the data of figure 5 is in principle easily extractible from the gauge theory. This demonstrates how from the gauge theory we can read off the details of the geometry deep inside the bulk. In other words,

---

[11]The two conditions can be distilled into a necessary condition for circular photon orbits; defining $Q(r) = \frac{1}{12}\rho(r)r^2 + 2\frac{m(r)}{r^2}$ we need $Q(r_0) = 1$ at some $r = r_0$. We find that $Q(r) \lesssim 0.6$ for all r irrespective of the internal density ρ_0.

just by looking at the spread of the endpoints of the null geodesics, we can distinguish the star from a small black hole (as demonstrated below) or other configurations of the same mass in AdS. Note that this is rather different method of extraction of details of deep IR in the bulk from that employed in [16]: the latter considered one-point functions, whereas here we make explicit use of the nonlocal nature of the two-point functions.

3.3 Field theory signature of excited AdS geometries

We now turn to a brief analysis of the star geometry from a field theory perspective. By construction we have an asymptotically AdS geometry which is static and spherically symmetric. While we have modeled the star by an effective equation of state, it is easy to see that similar solutions can be obtained in gauged supergravity theories. In any event the geometries in question correspond to normalizable deformations of the AdS vacuum, implying that they are dual to states in the field theory. In particular, these states should be eigenstates of the CFT Hamiltonian (since they are static). One can therefore use the state operator correspondence in the CFT to map the state into an operator insertion; for convenience we will call the state of the star $|star\rangle$ and the corresponding operator $\mathcal{O}_*$ *i.e.*, $|star\rangle = \mathcal{O}_* |0\rangle$. Note that to obtain a geometry with spherical symmetry we would need to smear the operator insertion $\mathcal{O}_*$ on the boundary $\mathbf{S}^3$ making it effectively non-local.

One of the interesting questions that we will be unable to provide a concrete answer for is the precise description of the state $|star\rangle$ in the field theory. From general arguments it is clear that the operator $\mathcal{O}_*$ has dimension of $\mathcal{O}(N^2)$ in the field theory.[12] In order to ascertain the precise state we need more information than the one point function of the stress tensor (which is of course given by the leading fall-off in the metric). However, it is clear that on physical grounds such states ought to be constructible in the field theory and we will proceed with the assumption that $\mathcal{O}_*$ is a *bona fide* operator in the field theory.

Our analysis of geodesics in the star spacetime can be rephrased in light of the discussion in section 2 as predictions for new 'light-cone' singularities in the boundary correlators in the state $|star\rangle$. The later arrival at the boundary of radial null geodesics indicates that correlation functions of generic operators $\mathcal{O}$ in the field theory, $\langle star| \mathcal{O}(x) \mathcal{O}(y) |star\rangle$ will have singularities at $\Delta\varphi = \pi$ and Δt given by the appropriate time delay. Similarly, the implication of bulk Type $\mathcal{B}$ geodesics with angular momentum is that we will have light-cone singularities in field theory correlators at operator insertion points x, y such that $t_x - t_y = \Delta t$ and $\Omega_x - \Omega_y = \Delta\varphi$ with Δt and $\Delta\varphi$ given by the geodesic analysis.

While we have emphasized the results here as predictions for the gauge theory correlation functions in an excited state at strong coupling, we believe that some of these predictions can be tested. For instance, one can consider the 1/2 BPS states in $\mathcal{N} = 4$ SYM. The geometries dual to these states are explicitly constructed in [17]. Within this class of geometries one can focus on those which are asymptotically AdS and calculate the bulk prediction for the light-cone singularities using the nature of bulk geodesics. To compare with the field theory result we need to know the behavior of four point functions,

---

[12]This is because of the state being dual to a configuration of finite ADM mass M and the fact that the bulk Newton's constant scales like N^2.

which can be analyzed in large N perturbation theory (at weak coupling) by taking the probe operators to also be chiral primary. We hope to report on this in the near future.

4. Eternal black holes in AdS

In the previous section we discussed the behaviour of geodesics in spacetimes which are deformations of AdS, focussing on globally static geometries. We will now consider spacetimes such as the eternal Schwarzschild-AdS black hole which is causally nontrivial and not globally static. In this case we know that a large Schwarzschild-AdS black hole corresponds to a thermal state in the field theory. The analysis of geodesics will lead to interesting signatures of the black hole geometry which will be visible in thermal correlation functions.

4.1 Schwarzschild-AdS black hole: Structure of spacelike and null geodesics

We will first describe the structure of null and spacelike geodesics in an AdS black hole background. Again focusing attention on 5-dimentional AdS, the black hole metric is given by

$$ds^2 = -f(r)\, dt^2 + \frac{1}{f(r)} dr^2 + r^2\, d\Omega_3^2 \tag{4.1}$$

with

$$f(r) = r^2 + 1 - \frac{\mu}{r^2} \; . \tag{4.2}$$

The mass of the black hole is proportional to μ, and correspondingly the horizon radius r_+ and the inverse Hawking temperature β are given by[13]

$$r_+^2 = \frac{\sqrt{1 + 4\mu} - 1}{2}, \qquad \beta = \frac{2\pi\, r_+}{2\, r_+^2 + 1} \; . \tag{4.3}$$

The equations for general geodesics are given as:

$$\dot{t} = \frac{\alpha}{f(r)} \; , \qquad \dot{\varphi} = \frac{1}{r^2} \; , \qquad \text{and} \;\; \dot{r}^2 = \alpha^2 - V_{eff}(r) \; , \tag{4.4}$$

where

$$V_{eff}(r) = -\frac{\kappa}{J^2}\, f(r) + \frac{f(r)}{r^2} \tag{4.5}$$

and $\kappa = 1, 0,$ or -1 for spacelike, null, or timelike geodesics, respectively, and the dot denotes differentiation with respect to the affine parameter along the geodesic.

Null geodesics in the black hole background ($\kappa = 0$) are parameterized by the ratio $\alpha = \frac{E}{J}$. Once again we will be interested to know which points are connected by bulk null geodesics and we will quantify this in terms of $(\Delta t(\alpha), \Delta \varphi(\alpha))$. The radial equation is easy to interpret as a classical particle with energy α^2 moving in a potential $V_{eff}(r) = \frac{f(r)}{r^2}$ (see figure 6). $V_{eff}(r)$ has a maximum at $r_m^2 = 2\mu$ with a value $V_{eff}(r_m) = 1 + \frac{1}{4\mu}$ and as $r \to \infty$, $V_{eff} \to 1$. The null geodesics connecting boundary points are:

---

[13]Note that to describe a big black hole we need $\mu \geq \frac{3}{4}$. Further, for the temperature of the system to be high enough so that the big black hole dominates the thermal ensemble, we require $\mu \geq 2$, which corresponds to $T = \frac{1}{\beta} \geq \frac{3}{2\pi}$. For illustration, we often use an example with $\mu = 1$ below.
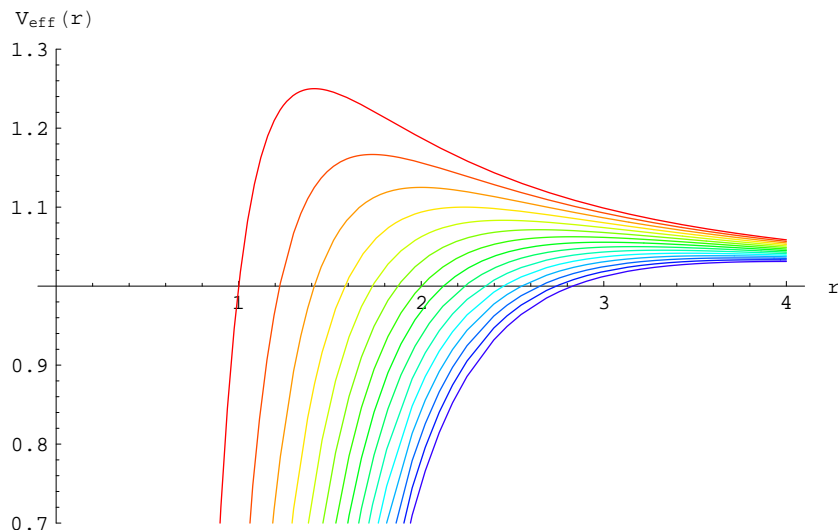
Figure 6: The plot for $V_{eff}(r) = f(r)/r^2$ for $\mu \in \{1, 1.5, 2, \cdots, 7.5, 8\}$.

1. Geodesics with $\alpha = 1$, *i.e.*, $E = J$, stay at constant $r = \infty$; these are null geodesics of the boundary manifold (Type $\mathcal{A}$).

2. The null geodesics which pass into the bulk and come back to the boundary (Type $\mathcal{B}$) exist only for $\alpha \in (1, \alpha_0)$, where

$$\alpha_0^2 = V_{eff}(r_m) = 1 + \frac{1}{4\mu} \tag{4.6}$$

As $\alpha \to 1$, we find that $(\Delta t, \Delta \varphi) \to (\pi, \pi)$. It is also clear from figure 6 that as $\alpha \to \alpha_0$, $\Delta t(\alpha)$ and $\Delta \varphi(\alpha)$ should go to infinity since it takes infinite affine parameter time to reach the turning point.[14] One can further check that

$$\alpha \frac{dt}{d\alpha} = \frac{d\varphi}{d\alpha} \qquad \Longrightarrow \qquad \frac{d\varphi}{dt} = \alpha(t). \tag{4.7}$$

From this we conclude that as $\alpha \to \alpha_0$,

$$\Delta t(\alpha) \approx \frac{1}{\alpha_0} \Delta \varphi(\alpha) \to \infty \tag{4.8}$$

Note that since $\alpha_0 > 1$, the above equation implies $\Delta t < \Delta \varphi$. This remains true for general values of $\alpha \in (1, \alpha_0)$ as is clear from figure 7, which is a parametric plot of $\Delta \varphi(\alpha) - \Delta t(\alpha)$ by varying α. Note that since φ is periodic, there is no violation of causality here.

In order to better understand the set of boundary points that can be connected through the bulk, we should also look at spacelike geodesics, which are discussed in detail in appendix C.

---

[14]Or said differently, as $\alpha \to \alpha_0$, the geodesic can go around the circular orbit at $r_m = \sqrt{2\mu}$ many times before re-escaping to the boundary.
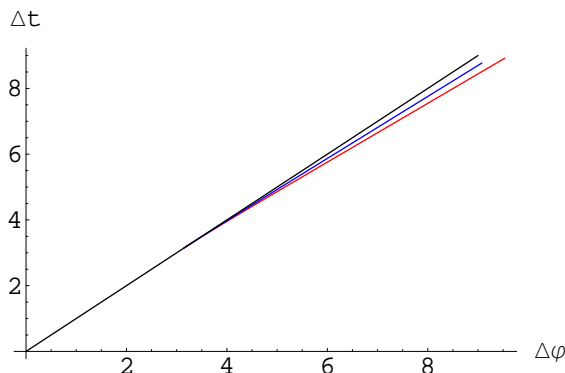
Figure 7: End points of null geodesics in a black hole background. The black line is $\Delta t = \Delta \varphi$, which is the set of end points of boundary null geodesics. The blue and red curves give the end points of bulk null geodesics for a black hole with $\mu = 2$ and $\mu = 1$, respectively. It is obtained by varying $\alpha \in (1, \alpha_0)$. As $\alpha \to 1$, $(\Delta t, \Delta \varphi) \to (\pi, \pi)$ and as $\alpha \to \alpha_0$, Δt and $\Delta \varphi$ approach infinity with their ratio given by $1/\alpha_0$. Note that $\Delta \varphi(\alpha) > \Delta t(\alpha)$ for $\alpha \in (1, \alpha_0)$.

4.2 New singularities for thermal YM theories on $\mathbf{S}^3$

We now consider gauge theory implications of the null geodesics in the black hole background. As discussed in section 2, we will assume that null geodesics lead to the singularities of boundary correlation functions.

At a spatial point $\Delta \varphi = \varphi_0$, boundary null geodesics will give rise to singularities at

$$\Delta t = \varphi_0, \ \varphi_0 + 2\pi, \ \varphi_0 + 4\pi, \cdots . \tag{4.9}$$

These are singularities of vacuum correlation functions and we expect they survive at finite temperature as well. Type $\mathcal{B}$ null geodesics which go into the bulk will give rise to new singularities at

$$\Delta t_1 = \varphi_0 + 2\pi \, b_1(\varphi_0), \ \Delta t_2 = \Delta t_1 + 2\pi \, b_2(\varphi_0), \ \cdots , \ \Delta t_n = \Delta t_{n-1} + 2\pi \, b_n(\varphi_0), \ \cdots , \tag{4.10}$$

where Δt_n, $n = 1, 2, \cdots$ are obtained by the intersection of the red line with vertical lines $\Delta \varphi = 2\pi n + \varphi_0$ in figure 7. Here $b_n(\varphi_0)$ is some number lying between $1/\alpha_0$ and 1 and is smaller than 1. As n becomes large,

$$b_n(\varphi_0) \to \frac{1}{\alpha_0} = \frac{1}{\sqrt{1 + \frac{1}{4\,\mu}}} \tag{4.11}$$

independent of the value of φ_0. The locations of these singularities are temperature-dependent, since α_0 and b_n depend on the temperature of the system (through μ). Since all b_n are smaller than 1, the singularities in (4.10) are generically distinct[15] from those in (4.9). Note as we increase the temperature of the system (*i.e.*, increase the black hole mass μ), $\alpha_0 \to 1$ and the two sets of singularities merge in the $\mu \to \infty$ limit. In the high temperature limit, $\mathbf{S}^3$ effectively decompactifies to $\mathbf{R}^3$, and as we discussed earlier there

---

[15]At some special values of φ and t, it is possible for them to coincide.

are no bulk null geodesics in this limit (see appendix D) when we insist on maintaining the Poincaré symmetry.

Since "new" singularities arise from null geodesics which go into the bulk, they encode information regarding the bulk geometry. That singularities exist for $\Delta t \to \infty$ is a reflection of the existence of a (unstable) circular orbit at $r_m = \sqrt{2\mu}$ in the bulk geometry. The time difference $\Delta t_n - \Delta t_{n-1}$ between nearby singularities for n large is simply given by the time that it takes a null geodesic to traverse the circular orbit (which is $2\pi/\alpha_0$). More generally, denoting the locations of the singularities by the curve $\Delta t(\Delta\varphi)$, from the second equation of (4.7) it follows that the slope $\frac{d\Delta t}{d\Delta\varphi}$ gives $1/\alpha = J/E$ of the corresponding bulk geodesic.

Also note that in cases where the bulk geometry deviates from that of the Schwarzschild-AdS geometry in the vicinity of the horizon, such as the smooth microstate geometries discussed in the context of D1-D5 systems (*cf.*, [18, 19] for reviews and references), the gauge theory should in principle be able to detect even slight deviations which cause a slight shift in the radius of the null circular orbit. This is facilitated by the fact that the slope $\frac{d\Delta t}{d\Delta\varphi}$ can be measured arbitrarily precisely for large enough separations Δt and $\Delta\varphi$.

Our conclusion above was obtained in the supergravity limit, *i.e.*, large N and large λ limit. It would be interesting to understand whether the "new singularities" at finite temperature arise when one departs away from the limit. In particular, it would be interesting if one could find independent arguments for their existence in the gauge theory.

5. Horizon formation from gauge theories

In the preceding sections we have focused on static[16] bulk geometries and indicated how to extract certain details about the geometry from the boundary correlators. In this section we finally apply the relation between null geodesics and singularities of boundary correlators to the fully dynamical case of gravitational collapse. Previous studies of black hole collapse in the AdS/CFT context are [20 – 23].

The basic question we want to ask is: *Can we see horizon formation directly in the gauge theory?* Since in the bulk, horizon formation is a sharply-localized event (despite the fact that we need to know the full future evolution of the spacetime to actually find the horizon), we would expect that there will correspondingly be some sharp feature in the gauge theory. We will start by considering the simplest toy model, which is that of a collapsing spherical null shell. However, our main result should be applicable to general gravitational collapse, as will be clear below.

5.1 Null geodesics in a gravitational collapse

Consider a null spherical shell in d-dimensional asymptotically AdS spacetime. We can take the metric inside and in the past of the shell to be pure AdS, and the metric outside and to the future of the shell to be Schwarzschild-AdS. The metrics for the interior and

---

[16]Although the eternal black hole spacetime is not globally static, the method sketched above only probed the static part of the geometry. We comment on extracting the details of the dynamic spacetime inside the horizon in appendix C.

the exterior of the shell can be written as

$$ds^2 = -f_{in,out}(r)\,dt^2_{in,out} + \frac{dr^2}{f_{in,out}(r)} + r^2\,d\Omega^2_{d-2} \tag{5.1}$$

where

$$f_{in}(r) = r^2 + 1 \tag{5.2}$$

$$f_{out}(r) = r^2 + 1 - \frac{\mu}{r^{d-3}} \ . \tag{5.3}$$

The mass of the black hole is proportional to μ. As in the previous section, we will use r_+ to denote the horizon radius and the surface gravity κ of the black hole is given by

$$\kappa = \frac{2\pi}{\beta} = \frac{1}{2}\frac{df_{out}}{dr}\bigg|_{r_+} \tag{5.4}$$

with β the inverse Hawking temperature. Note that the t coordinate jumps across the shell with the jump approaching zero at the boundary. In contrast, the r coordinate is physical (since it measures the proper area of the spheres in a spherically symmetric spacetime) and therefore varies continuously across the shell.

The Penrose diagram for the collapse is sketched in figure 8. There is only one asymptotic region; below the shell, the spacetime is pure AdS, whereas above, it is exactly Schwarzschild-AdS.[17] The two important times, which are labeled in figure 8 (a), are the time of the creation of the shell, t_s, and the time of the horizon formation. In global coordinates, the latter occurs in the bulk at the origin $r = 0$ at $t = t_H$; however, this need not correspond directly to the CFT time, since we're describing an event at $r = 0$ rather than at $r = \infty$. Instead, the important CFT time related to the horizon formation is given by $t = t_h$ (labeled on the boundary), which is the time from which a radial null geodesic would have to start in order to hit the horizon formation event ($r = 0, t = t_H$).

Since this is a time-dependent geometry, the behavior of a null geodesic depends on the time t_i of the initial point. Radial null geodesics therefore separate into three qualitatively distinct classes, indicated in figure 8 (b):

  I. For $t_i < t_s - \pi$, the geodesic is given by that of the pure AdS, and $t_o < t_s$.

 II. For $t_s - \pi < t_i < t_h$, the geodesic starts out in AdS, crosses the shell at some point outside the horizon, and continues in Schwarzschild-AdS, reemerging to the boundary at $t_o \in (t_s, \infty)$.

III. For $t_h < t_i < t_s$, the geodesic starts out in AdS but crosses the shell at some point inside the horizon, and therefore hits the singularity (the last part of the geodesic III sketched in figure 8 (b) pertains to nearly null spacelike geodesics which can bounce off the singularity). For $t_i > t_s$, the radial null geodesic starts out in Schwarzschild-AdS and therefore crashes into the singularity; whereas for the nearly-null spacelike geodesics, this case is already covered above by reversing the orientation.

---

[17]The singularity is drawn with a tilt for more realistic representation of the Penrose diagram in $d > 3$ dimensions (the shape of the singularity depends on d and r_+); however, here the "Penrose diagram" is to be treated as a sketch for ease of visualisation rather than an exact causal diagram.
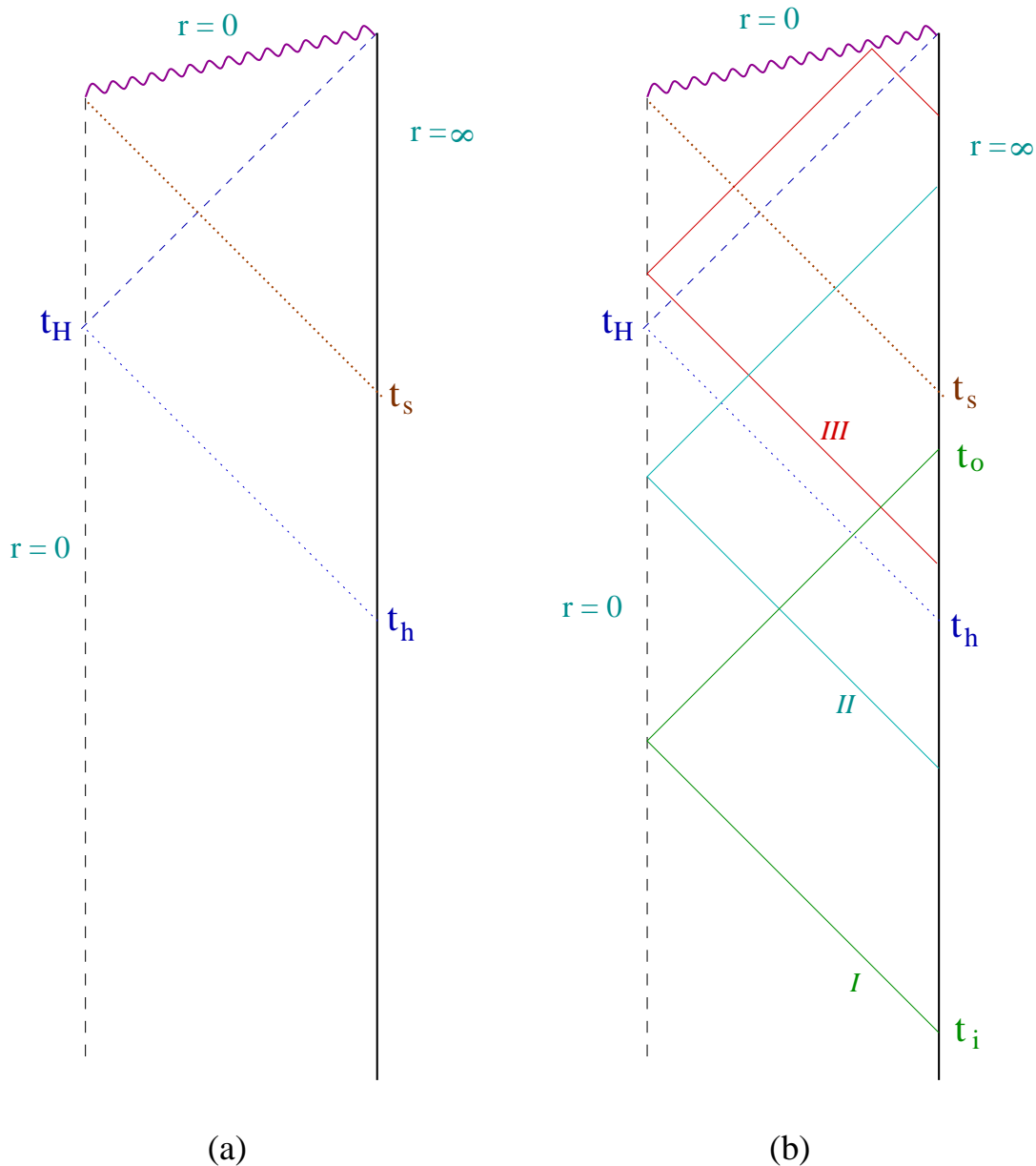
Figure 8: Penrose diagram for a collapsed black hole. **(a)** shows the times for the shell creation and horizon formation; **(b)** in addition illustrates three distinct regimes of radial null geodesics. (Note that the last (upper right) part of geodesic *III* is only relevant for nearly-null spacelike geodesics which can bounce off the singularity. Also, to avoid cluttering the diagram, the starting time t_i and ending time t_o are labeled only for geodesic *I*.)

We discussed geodesics in AdS and Schwarzschild-AdS spacetimes in previous sections; here we match them together to analyse the behaviour in the collapse geometry. We focus on null geodesics of Type $\mathcal{B}$, with $t_i \in (t_s - \pi, t_h)$; this will be the interesting regime where we can probe the event horizon formation. Note that $t_h \in (t_s - \pi, t_s)$, with t_h occurring earlier for larger black hole. In particular, using ray tracing within the AdS spacetime one

can show that the horizon formation time is related to the shell creation time t_s and its mass, or equivalently r_+, by (see appendix E for a derivation)

$$t_h = t_s - 2 \tan^{-1} r_+ \ . \tag{5.5}$$

Let us first consider radial null geodesics. From the Penrose diagram, it is clear that as $t_i \to t_h$ from below, $t_o \to \infty$, while for $t_i > t_h$, the null geodesic falls into the singularity and does not come back to the boundary. Since this will constitute the sharp CFT signature of the horizon formation event in the bulk, let us examine this feature in greater detail. The manner in which t_o diverges as $\delta t \equiv t_h - t_i \to 0^+$ can be obtained by following Hawking's ray tracing argument [24], which gives

$$t_o \approx -\frac{1}{\kappa} \log \delta t + \text{constant} \qquad \Longrightarrow \qquad \delta t \sim e^{-\kappa t_o} \tag{5.6}$$

where κ is the surface gravity of the black hole.[18] To see (5.6), consider a point P_+ on the horizon just outside the shell. Let v^μ to be the vector tangent to the horizon at P_+ and u^μ be the null vector directed normally outward from the horizon normalized so that $u \cdot v = 1$. The vector at P_+ which connects the horizon with the null geodesic can thus be written as ϵu^μ for some ϵ. As $t_o \to \infty$, ϵ can be expressed in terms of t_o as

$$\epsilon \approx A e^{-\kappa t_o}, \qquad t_o \to \infty \tag{5.7}$$

with A some constant independent of t_o. Now parallel transport u^μ and v^μ across the shell to the point P_- on the horizon just inside the shell.[19] ϵ remains invariant under this transformation. At P_- one can express ϵ in terms of δt as

$$\epsilon \approx B \, \delta t \tag{5.8}$$

with some constant B. Comparing (5.7) and (5.8), we obtain the desired relation (5.6).

Note that the leading behavior (*i.e.*, the logarithmic dependence) in (5.6) is rather robust, independent of the collapsing configuration and the type of black hole formed (charged, rotating). In appendix E we also give alternative derivation of (5.6) for some explicit examples. While our arguments so far were of a qualitative nature, we can make rather precise predictions for where the singularity in the collapse state correlators should appear. This is carried out in some detail in appendix E, where we calculate t_o in terms of t_i and the parameters describing the state, t_s, r_+, and κ, to be

$$t_o = t_s + \frac{2}{r_+ \kappa} \left((1 + r_+^2) \frac{\pi}{2} - (1 + r_+^2) \tan^{-1} \frac{r_c}{1 + r_+^2} + r_+ \tanh^{-1} \frac{r_c}{r_+} \right) \tag{5.9}$$

where r_c denotes the crossing radius where the geodesic intersects the shell, $r_c = \tan \left(\frac{t_s - t_i}{2} \right)$.

To summarize, we find that radial null geodesics are sensitive probes of horizon formation. The infinite redshift at the horizon translates into a sharp time scale t_h (5.5) at the boundary.

---

[18]Intuitively Eq.(5.6) reflects the fact that the redshift experienced by the outgoing null ray increases exponentially with t_o as $e^{\kappa t_o}$ when $t_o \to \infty$.

[19]Note that u^μ and v^μ are continuous when crossing the shell.

Now let us consider non-radial null geodesics. A natural question is whether there exists an analogous value $t_h(\alpha)$ for each[20] $\alpha = E/J$ so that as $t_i \to t_h(\alpha)$, the corresponding $t_o \to \infty$. The answer turns out to be yes for a range of values of α, but for a different reason from that for the radial geodesics. By the very nature of an event horizon, we expect that the only null geodesic which truly samples the event horizon formation is the radial one; any other null geodesic which approaches the horizon non-radially cannot escape to the boundary. In appendix F, we describe how to compute $t_h(\alpha)$ for general α. We show that all geodesics with angular momentum for which t_o diverges take that long to reach the boundary not because of being trapped near the event horizon, but rather because of circling around a null circular orbit at a given finite distance outside the horizon.

It is easy to see that $t_h(\alpha)$ depends non-trivially on α; the presence of angular momentum causes the geodesic to sample a different region of the spacetime geometry. In the limit $\alpha \to 1$ (maximal angular momentum) we expect that the geodesic stays arbitrarily close to the boundary, so that it doesn't sample the black hole geometry, and in particular there can be no divergence in t_o for any finite t_i. In the opposite limit of zero angular momentum, we have already seen that $t_h(\infty)$ is given by the expression for t_h for the radial geodesic (5.5). The result of appendix F is summarized in figure 9, which plots $t_h(\alpha)$ as a function of $J \sim 1/\alpha$. In particular, we note that:

$$
\begin{aligned}
t_h(\alpha) &\to t_h = t_s - 2\tan^{-1}(r_+) , \qquad \alpha \to \infty \\
t_h(\alpha) &\to t_s , \qquad \alpha \to \alpha_0
\end{aligned}
\tag{5.10}
$$

while for $1 < \alpha < \alpha_0$, t_o never diverges, where α_0 was introduced in (4.6). Recall that the Schwarzschild-AdS geometry contains a null circular orbit with $\alpha = \alpha_0$ at $r = \sqrt{2\mu}$. As figure 9 demonstrates, $t_h(\alpha)$ is not a monotonic function of $1/\alpha$. In particular, the minimal value of $t_h(\alpha)$, which we will denote as t_c, is smaller than t_h, the horizon formation time. t_c is the boundary time scale at which the null circular orbit of the newly formed black hole geometry is first probed.

In figure 10, we plot the endpoints of various geodesics on the $\Delta t - \Delta\varphi$ plane[21] for a fixed initial time $t_i \in (t_s - \pi, t_s)$. Note that in contrast to the analogous plots in earlier sections for other geometries, the background here does not have a time translational symmetry. For ease of visualization we unwrap the φ direction and at the same time compactify both the Δt and $\Delta\varphi$ so that we can examine the full $\Delta t - \Delta\varphi$ plane. For each fixed t_i, we plot the end-point curve, color-coded by α. For $t_i < t_s - \pi$, the endpoints would all clump into the single point $(\Delta\varphi, \Delta t) = (\pi, \pi)$. As we increase t_i so that the geodesics start sampling the shell, the endpoints begin to spread in the manner shown on the left in figure 10, into a cusp similar to the star geometry (cf. figure 5). As t_i reaches the minimum of the curve $t_h(\alpha)$ shown in figure 9 (i.e., $t \to t_c$), the cusp extents to $(\Delta\varphi, \Delta t) = (\infty, \infty)$ (upper right

---

[20]Since the shell geometry is not static, E jumps across the shell; in defining α we use the initial E i.e., its value in pure AdS.

[21]Since α is the only continuous free parameter describing the null geodesics, this will produce a curve of endpoints on the $\Delta t - \Delta\varphi$ plane.
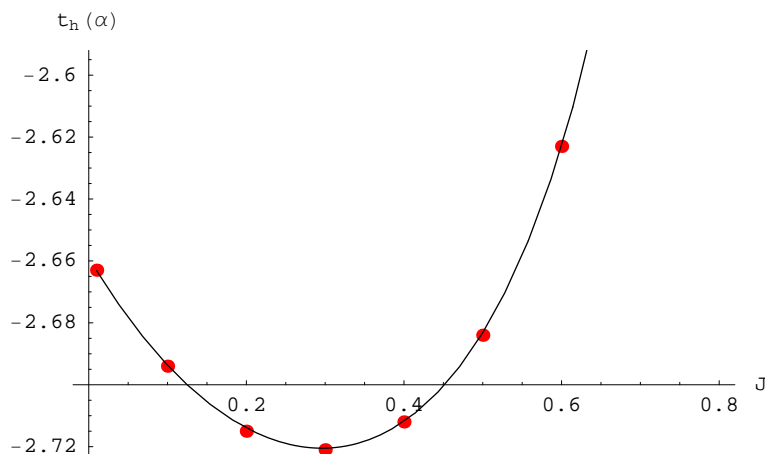
Figure 9: Variation of $t_h(\alpha = \frac{1}{J})$ as a function of angular momentum J in the thin shell spacetime (5.1) (solid line). The intersection of the curve with vertical axis gives t_h, while the minimum gives t_c. Red dots are data extracted from figure 11, which were obtained by numerical integration of the geodesics in the Vaidya spacetime (5.12), (5.13) with $v_s = 0.001$.

corner of the plots) with

$$\Delta t(\alpha) \approx \frac{1}{\alpha_0} \Delta\varphi(\alpha) \to \infty \ . \tag{5.11}$$

Increasing t_i further, the cusp still reaches $(\Delta\varphi, \Delta t) = (\infty, \infty)$ with (5.11), but now for two different values of α, given by solution to $t_h(\alpha) = t_i$. At the same time, Δt for the radial geodesic increases, diverging as $t_i \to t_h$. This will appear in figure 10 as the left end point of the upper branch moving to (π, ∞). The right plot in figure 10 is taken for t_i slightly smaller than t_h. Note that equation (5.11) follows from the fact that as $t_i \to t_h(\alpha)$, the geodesic goes around the circular null orbit with a period $\frac{2\pi}{\alpha_0}$ infinitely many times.

One can generalize the sharp shell to a smeared-out version which is physically more realistic. To that end, we consider a Vaidya spacetime of the form

$$ds^2 = -f(r, v)\, dv^2 + 2\, dv\, dr + r^2\, d\Omega_3^2 \tag{5.12}$$

with $f(r, v)$ smoothly transitioning between (5.2) at $v \to -\infty$ and (5.3) as $v \to +\infty$; a convenient form to use is

$$f(r, v) = r^2 + 1 - \frac{\mu}{r^2}\left(\frac{1 + \tanh\frac{v}{v_s}}{2}\right) \tag{5.13}$$

In particular, the shell is inserted at $v = 0 = t_s + \pi/2$, and has 'thickness' v_s. As $v_s \to 0$, we recover the collapse spacetime (5.1) written in ingoing coordinates.

Figure 11 shows the value of $\Delta t = t_o - t_i$ for a set of non-radial geodesics in the spacetime (5.12) with various values of α, all starting at the initial time t_i; in (a) the shell is very thin whereas in (b) the shell is considerably smeared out. The value of $t_h(\alpha)$ can be read off from the plot; it corresponds to the value of t_i at which Δt diverges for a geodesic with that α. For the thick shell in figure 11 (b), we see that these times are well-separated, and increase monotonically with increasing J/E (decreasing α).
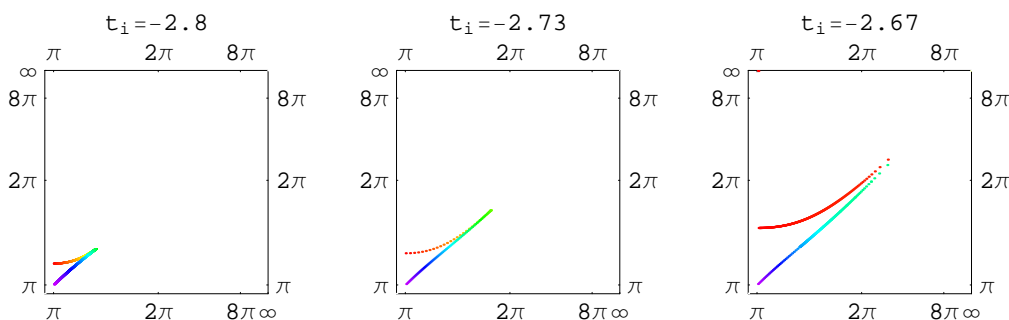
Figure 10: Plot of $(\Delta\varphi, \Delta t)$ for 3 values of t_i in the thin shell geometry (same configuration as in figure 9 and figure 11(a)), for various values of $\alpha \in (1, \infty)$. The horizontal and vertical axes show $\Delta\varphi$ and Δt respectively, rescaled by $\tan^{-1}$ to fit the full plane. The left endpoint of the upper branch corresponds to $\alpha = \infty$ (radial geodesic), while the left endpoint of the lower branch corresponds to $\alpha = 1$. (a) $t_i = -2.8 < t_c \approx -2.72$; (b) $t_i = -2.73$ only slightly smaller than t_c; (c) $t_i = -2.67$ slightly smaller than $t_h \approx -2.66$. Here t_c is the minimal value of the curve in figure 9 and t_h is intersection of the curve in figure 9 with the vertical axis. As $t_i \to t_c$ the cusp should reach (∞, ∞) (upper right corner) and as $t_i \to t_h$, the left endpoint of the upper branch should reach (π, ∞) (the upper left corner). Note that as apparent from figure 11, the endpoints vary rather sharply with t_i for $t_i \approx t_h(\alpha)$, so it is difficult numerically to sample the large values of $\Delta\varphi, \Delta t$.
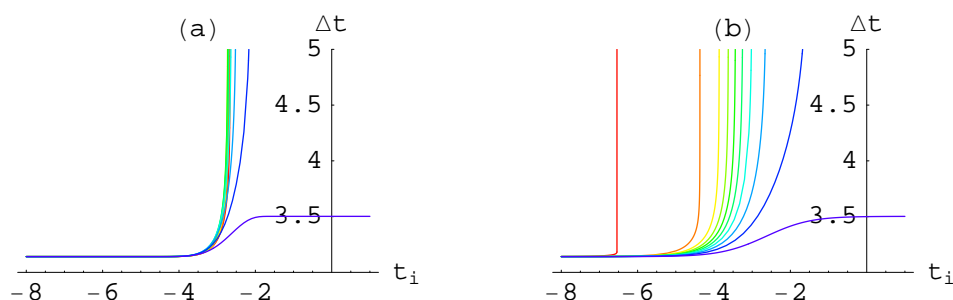

Figure 11: Plot of Δt as a function of t_i for non-radial null geodesics in the Vaidya metric with the effective "thickness" of the shell given by **(a)** $v_s = 0.001$ and **(b)** $v_s = 1$. The various curves differ[ent] angular momenta, $J = 0.01, 0.1, 0.2, 0.3, \ldots$.

This illustrates that the sharp signature of the horizon formation event is not limited to the thin-shell collapse (bulk spacetimes with a null shell sharply separating pure AdS from Schwarzschild-AdS): For any spherically symmetric spacetime in which an event horizon forms at a time t_H at the origin, reachable by an ingoing radial null geodesic starting at the boundary at t_h, we can find t_h by exactly the same method. In particular, our method constitutes following the red (leftmost) curve in figure 11 (b).

To summarize, whereas only the radial null geodesic starting at t_h samples the horizon formation event, the non-radial null geodesics provide further details about the geometry, in particular the null circular orbit of the newly formed black hole geometry. Furthermore the variation of the curves $\Delta t(\Delta\varphi)$ with respect to t_i provides spatio-temporal information both dynamically around the horizon formation time and spatially in the vicinity of the

horizon.

5.2 Gauge theory signatures

We can now translate the behaviour of null geodesics in the bulk collapse spacetime to predictions regarding boundary correlation functions. Our discussion below should apply to generic highly excited states in the boundary theory[22].

Consider the CFT correlators of the form $\langle \mathcal{O}(t_i, \Omega) \, \mathcal{O}(t_o, -\Omega) \rangle_{\text{shell}}$ evaluated explicitly in the state of the shell. Modelling the shell as being created by an operator $\mathcal{S}$ inserted in the boundary at $t = t_s$, we have

$$
\begin{aligned}
\langle \mathcal{O}(t_o, \Omega') \, \mathcal{O}(t_i, \Omega) \rangle_{\text{shell}} &= \langle 0 | \, \mathcal{O}(t_o, \Omega') \, \mathcal{O}(t_i, \Omega) \, | 0 \rangle \, , && t_i < t_o < t_s \\
&= \langle 0 | \, \mathcal{O}(t_o, \Omega') \, \mathcal{O}(t_i, \Omega) \, \mathcal{S}(t_s) \, | 0 \rangle \, , && t_i < t_s < t_o \\
&= \langle 0 | \, \mathcal{S}^\dagger(t_s) \mathcal{O}(t_o, \Omega') \, \mathcal{O}(t_i, \Omega) \, \mathcal{S}(t_s) \, | 0 \rangle \, , && t_s < t_i < t_o
\end{aligned}
\tag{5.14}
$$

By our previous arguments, we would expect this correlator to become singular when the insertion points are connected by a null geodesic. More explicitly,

I. When $t_o < t_s$, the correlator is simply the standard vacuum two point function. The singularities are given by the usual light cone singularities of the boundary theory. As is clear from geodesic I in figure 8(b)), all null geodesics lie entirely in the AdS region.

II. When $t_i < t_s < t_o$, the correlator is given by the second line of (5.14). From our discussion of null geodesics in last subsection, the pattern of bulk-cone singularities for this correlator has a rich structure, which reflects the formation of the event horizon and the null circular orbit in the bulk.

Suppose experimentalists in the boundary theory are able to measure the observable $\langle \mathcal{O}(t_i, \Omega) \, \mathcal{O}(t_o, -\Omega) \rangle_{\text{shell}}$ for all t_i and t_o satisfying $t_i < t_s < t_o$. Then by carefully plotting the locations of singularities of the correlator in the $\Delta t - \Delta \varphi$ plane for a given t_i, they should recover various plots of figure 10. In particular two distinct time scales emerge by comparing the pattern of singularities for different t_i. The first is the time t_c when the cusp in figure 10 reaches (∞, ∞). This is the time scale that non-radial null geodesics originating from the pure AdS geometry start being trapped by the circular orbit of the newly formed black hole. The slope of the line reaching the infinity gives the period of the orbit. The second is the time t_h that the left end of the upper branch (which corresponds to radial geodesics) reaches (π, ∞). This is the time of horizon formation as probed by a radial null geodesic. The bulk time of horizon formation in global AdS coordinates is given by $t_H = t_h + \frac{\pi}{2}$.

III. When $t_s < t_i < t_o$, the correlator is given by the third line of (5.14). In this case, all singularities of the correlator are the same[23] as those of a finite temperature

---

[22]By highly excited states we mean states of energies of order cN^2, with N-independent constant c sufficiently big. By generic states we mean states which are generic superpositions of energy eigenstates. Note that energy eigenstates do not give rise to the desired time dependence.

[23]The correlator itself does not necessarily coincide with a thermal correlation function. Only the singularity structure does.

correlation function with the temperature T given by

$$\frac{1}{T} = \frac{\partial \log \Omega(E)}{\partial E} \tag{5.15}$$

where E is the energy of the shell state and $\Omega(E)$ is the density of states of the CFT. This follows from that all type $\mathcal{B}$ geodesics with $t_s < t_i < t_o$ are identical to those of an AdS black hole.

In the above we discussed the pattern of bulk-cone singularities of (5.14). There might also be more subtle signals, on a secondary sheet (so we would find the singularity in the correlator only after a suitable analytic continuation) when the insertions are separated by a spacelike geodesic which is arbitrarily close to being null as illustrated for the eternal black hole singularity in [6]. In other words, the corresponding geodesic passes through the black hole and bounces off the singularity[24], see e.g. geodesic III of figure 8(b). Such a situation could arise when $t_i > t_h$ (which, if we define $t_i < t_o$, also implies that $t_i < t_s < t_o$). We will discuss it in more detail in section 5.3.

5.3 Signature of the black hole singularity?

In addition to the null geodesics considered in figure 8, it is also of interest to consider some spacelike geodesics. In particular, spacelike geodesics have the important feature that they 'bounce off' the black hole singularity [6], and thus could provide valuable information about the black hole singularity. There are two other types spacelike geodesics in the collapse background which are of particular interest (see figure 12):

1. $t_i \to t_h$ from above and $t_o \to \infty$. As can be seen from Fig.12a, the geodesic passes inside the horizon and bounces off the singularity. We will calculate below the dependence of t_o on $\delta t = t_h - t_i$.

2. As $t_i \to t_s$, $t_o \to t_s$. The corresponding geodesic is sketched in figure 12b. One expects that $t_o - t_s \sim (t_s - t_i)^\gamma$, where γ should depend on how strongly geodesics are repelled from the singularity.

Note that spacelike geodesics are parameterized by E and J, but here we set $J = 0$ to focus on radial geodesics, and moreover we take the infinite E limit, so that their trajectories converge to the radial null geodesics, except for the important point that they 'bounce off' the black hole singularity. As before, we can find geodesics in the full collapsing geometry by patching the geodesic segments in the respective regions; here in addition to AdS (region 1 in figure 12c) and the Schwarzschild-AdS region outside the horizon (region 2 in figure 12c), we now have to consider Schwarzschild-AdS inside the horizon as well (region 3 in figure 12c). This is presented in detail in appendix E; here we only quote the main results.

1. As $t_i \to t_h^+$, $t_o \to \infty$ in the same manner as for $t_i \to t_h^-$ (*cf.* Eq.(5.6)), namely:

$$-\delta t = t_i - t_h \sim e^{-\kappa t_o} \tag{5.16}$$

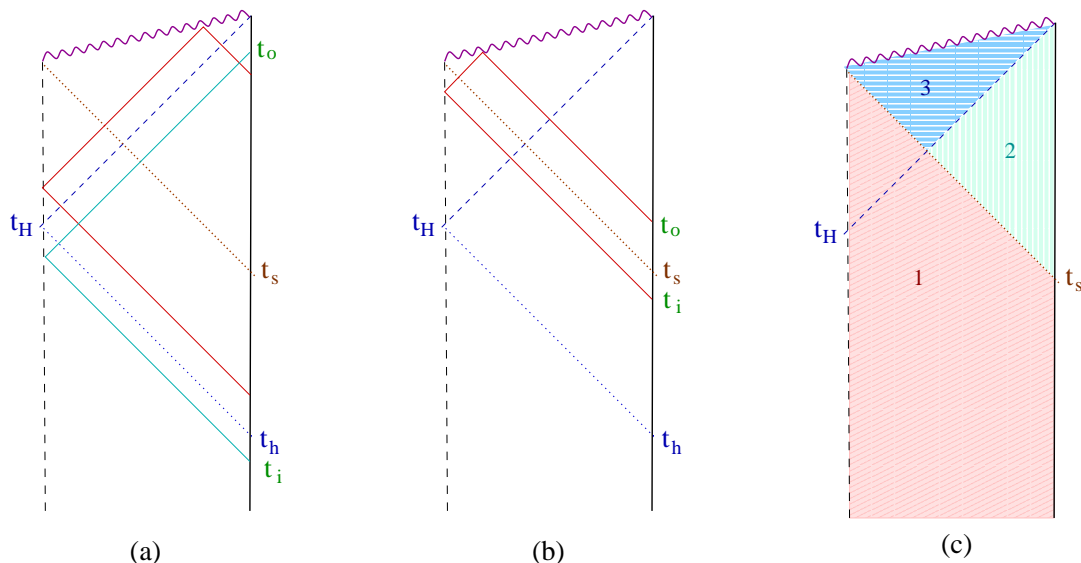[24]However, note that there is no longer a single radial null geodesic connecting the insertion points.

Figure 12: Penrose diagram for a collapsed black hole.

2. Let $t_s - t_i \equiv \varepsilon$. Then expanding $t_o - t_s$ to third order in ε, we find that

$$t_o - t_s \sim \varepsilon^3 . \tag{5.17}$$

with a coefficient which depends on the parameters of the final black hole – see (E.16).

As argued around (5.6), it is clear that the behaviour (5.16) is robust and is expected to hold in any spacetime dimension. The behaviour of the geodesic which bouces off the singularity in figure 12b, and in particular the exponent γ, depends crucially on the dimension; $\gamma = d - 2$ in AdS_d. Intuitively this is due to the fact that the curvature of the singularity increases with spacetime dimension.

6. Discussion

We have argued that the AdS/CFT correspondence implies the existence of "bulk-cone singularities" in boundary theory correlation functions, which lie inside the light-cone. The pattern of singularities can in turn be exploited to extract information about the bulk geometry. Our argument revolved around the essential point that Green's functions for quantum fields in curved space are singular when the arguments are null separated. While the geodesic approximation was necessary to derive the conclusion, we should point out that one expects the result to be true as long as it makes sense to talk about the spacetime geometry. In other words, we expect validity in α' expansion, but not necessarily in g_s expansion (where it is plausible to have a breakdown of the geometric picture).

We have demonstrated the pattern of singularities in the field theory correlators for several distinct scenarios: in radiation star, eternal Schwarzschild-AdS black hole, and the geometry of a collapsing shell. We have seen that small deformations of bulk geometries can in principle produce significant differences in the structure of singularities which are

discernible on the boundary. In this context it is also satisfying that the vacuum state of the CFT, corresponding to pure AdS spacetime, has a distinguished role, as evidenced by the theorem of [3]. Further, we are guaranteed that bulk-cone singularities for correlators evaluated in excited states occur at later times compared to the vacuum correlators, as necessitated by causality.

The novel application of our proposal was to the case of dynamical spacetimes. We concentrated on the simple scenario of a null shell collapse in AdS/CFT. One of the fascinating aspects of the singularity structure of the correlations is that they encode the spacetime event corresponding to event horizon formation in the bulk unambiguously. The characteristic signature we discussed is quite robust and can be easily distinguished from other singularities in the correlation functions. Further, the detailed pattern of singularities carries information about the geometry of the black hole that is formed. By using the non-local nature of the correlation functions we are able to extract information about the details of the bulk spacetime, while, in contrast to the recent discussions of probing the black singularity in AdS/CFT [6, 7], we are not reliant on analytic properties of the CFT correlators.

It would be very desirable to test our predictions of the existence of the bulk-cone singularities directly within the boundary theory. Note that the classical limit corresponds to the large N and large 't Hooft coupling limits of the boundary theory. It would be interesting to understand whether the appearance of bulk-cone singularities for correlation functions in excited states is an artifact of the large N and/or large 't Hooft coupling limits, or a generic feature for field theories on compact spaces.[25] Further, we expect that the semiclassical picture that we used in the bulk to be valid only in the large N limit – at any finite N we will have contributions from other semi-classical geometries that are sub-dominant saddle points of the quantum gravity path integral. In these circumstances it is not clear whether there is a precise meaning to the bulk light-cone. Nevertheless, we should note that the bulk-cone singularities discussed here are eminently trackable in the field theory even beyond the planar limit of large N. Understanding the role of these in some geometric terms is an interesting challenge.

An intriguing avenue to explore is to extend these considerations to "microstate geometries" proposed for black hole spacetimes. In situations where we have an explicit map between the spacetime geometries and the field theory states such as two charge D1-D5 system [18, 19], the 1/2 BPS sector of $\mathcal{N} = 4$ SYM [17], one can ask whether the pattern of singularities differs significantly between different states. The general arguments regarding the correlation functions of typical states that comprise the black hole entropy in [25 – 28] would seem to suggest that the structure of the singularities is not capable of discerning the fine distinctions between the geometries. This is however counter to the gravitational intuition: naively one expects geometries that differ from each other to have differing behaviour of Green's functions, especially with regard to the location of the singularities. A potential resolution of this discrepancy is that the geometric picture is incorrect for the

---

[25]Note that bulk-cone singularities do not arise for non-compact boundary as shown in appendix D for states preserving the boundary isometries.

"microstate geometries" as one has to consider a suitable wavefunction over the quantum moduli space of solutions. This is an interesting question that deserves to be explored further.

Another interesting generalization of our set-up would be to model the AdS/CFT analog of Choptuik scaling [29]. Given that we have a specific prediction for the field theory signature of black hole event horizon formation, one can ask whether the critical behaviour observed during the collapse has a field theoretic image and map out the details of the correspondence in this case.

Acknowledgments

A. Pure AdS

For ease of comparison of our results on the star and other geometries in what follows, we first summarise the basic facts regarding geodesics in AdS, concentrating on null and spacelike geodesics.

A.1 Geodesics in AdS: summary

Consider $d+1$-dimensional AdS in global coordinates. The metric can be written as

$$ds^2 = -f(r)\, dt^2 + \frac{dr^2}{f(r)} + r^2\, d\Omega_{d-1}^2$$
$$f(r) = 1 + r^2 \ . \tag{A.1}$$

The geodesic equations are as in (4.4), with $f(r)$ being that given in (A.1).

As we are primarily interested in the endpoints of null or spacelike geodesics (ultimately with diverging regularised proper length). To that end, the useful quantities are the temporal and angular separation of the geodesic endpoints, which we denote by Δt and $\Delta\varphi$, respectively. Let us first focus on spacelike geodesics, since as we will see, these limit to null geodesics. We can integrate the geodesic equations to obtain:

$$\Delta t = \frac{\pi}{2} + \sin^{-1}\left(\frac{E^2 - J^2 - 1}{e^{-L}}\right) \tag{A.2}$$

$$\Delta\varphi = \frac{\pi}{2} + \sin^{-1}\left(\frac{E^2 - J^2 + 1}{e^{-L}}\right) \tag{A.3}$$

$$e^{-L} = \sqrt{(E^2 - J^2)^2 + 2(E^2 + J^2) + 1} \tag{A.4}$$

where L is the geodesic length after regularising away the divergent piece $\log R_C^2$ (R_C is the radial cut-off). Finally, another useful expression is the minimum r value reached by the geodesic r_{min}

$$2\, r_{min}^2 = -(E^2 - J^2 + 1) + e^{-L} \tag{A.5}$$

From the expression for e^{-L} it is clear that we have a large negative length when

1. $E \to \infty$ with J fixed $\quad\Longrightarrow\quad L \sim -\log E^2$

2. $J \to \infty$ with E fixed $\quad\Longrightarrow\quad L \sim -\log J^2$

3. $J \sim E \to \infty \quad\Longrightarrow\quad L \sim -\log E$

Now consider two boundary points A and B are separated by boundary coordinate distance $\Delta t = \pi - \epsilon_t$ and $\Delta\varphi = \pi - \epsilon_\varphi$. We can easily see that for any spacelike separation $0 < \epsilon_{t,\varphi} < \pi$, there is a unique geodesic joining A and B; specifically we can calculate E and J for the geodesic given $\epsilon_{t,\varphi}$:

$$E = \frac{\sin \epsilon_t}{\cos \epsilon_\varphi - \cos \epsilon_t} \tag{A.6}$$

$$J = \frac{\sin \epsilon_\varphi}{\cos \epsilon_\varphi - \cos \epsilon_t} \tag{A.7}$$

and its length is

$$L = -\log 2 + \log(\cos \epsilon_\varphi - \cos \epsilon_t) \tag{A.8}$$

A.2 Spacelike $vs.$ null geodesics

Null geodesics in AdS only connect points with $\Delta t = \Delta\varphi = \pi$, irrespective of the parameter E/J. While this is a well known fact for radial null geodesics (for which $J = 0$), it is true that even geodesics carrying angular momentum emerge at the anti-podal point on the sphere in exactly AdS time. As mentioned in section 2 these null geodesics endpoints being coincident with the endpoints of purely boundary null geodesics, we do not see extra singularities in the correlation functions.

A naive puzzle about the null limit arises when we consider the difference between the angular separation of the endpoints $\Delta\varphi$ for spacelike and null geodesics. Spacelike geodesics in AdS allow any $0 \leq \Delta\varphi \leq \pi$; indeed for $E = 0$ (constant t slice) the geodesics plotted on the Poincare disk are circular arcs with diameter related to the angular momentum. On the other hand, null geodesics always reemmerge at the anti-podal point $\Delta\varphi = \pi$. How do the geodesics change their behaviour as we take $E \to \infty$ at fixed J? Figure 13 illustrates this limit. For any fixed finite J, as $E \to \infty$, we see that the geodesic indeed converges to the radial null geodesic and $\Delta\varphi \to \pi$.

Nevertheless, the full set of singularities of the boundary correlation function (2.10) is larger than those captured by the points with $\Delta t = \Delta\varphi = \pi$. It is interesting to ask whether there are any bulk geodesics (with divergent regularized proper length) that connect points
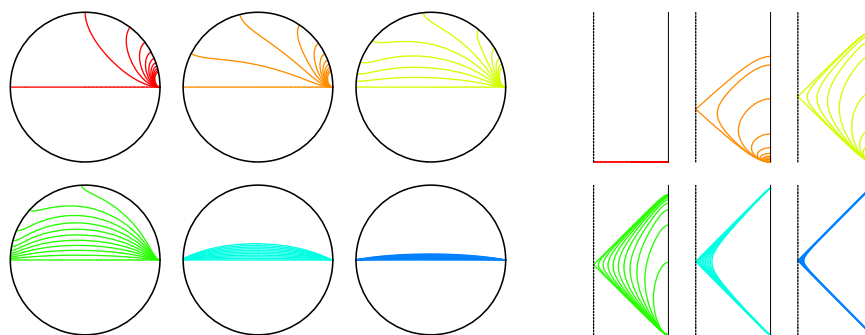
Figure 13: Spacelike geodesics in AdS, projected to a constant t slice (left) and the $t - r$ plane (right), for six different values of energy ($E = 0, 2, 5, 10, 30, 80$). For each E, geodesics with different values of angular momentum ($J = 0, 1, 2, \ldots, 10$) are plotted. The bold circles represent the boundary at $\tan r = \frac{\pi}{2}$. The dashed vertical lines correspond to the origin $r = 0$ and the bold vertical lines to the boundary at $\tan r = \frac{\pi}{2}$. The range of t plotted is $(0, \pi)$.

with $\Delta t = \Delta \varphi \neq \pi$. From (A.4), one concludes that the regularised proper length along a spacelike geodesic diverges not only when $E \to \infty$, but also when $J \to \infty$. Does this mean that this is an equally good null limit, and that therefore $\Delta \varphi = \pi$? The answer is no: as we can see from (A.3), as $J \to \infty$ at fixed E, $\Delta \varphi \to 0$. The geodesic has vanishing proper length because it is so short rather than because its tangent vector is null. On the boundary, this corresponds to the usual divergence of correlator of operators inserted at the same point.

However, it turns out that there nevertheless are nontrivial almost-null spacelike geodesics with $\Delta t = \Delta \varphi \neq \pi$. Consider spacelike geodesics in AdS parameterized by E and J with the following constraint:

$$J^2 = E^2 - \sigma E \tag{A.9}$$

for some real number σ. Upon taking the limit $E \to \infty$, we obtain

$$\Delta t \to \frac{\pi}{2} + \sin^{-1}\left(\frac{\sigma}{\sqrt{\sigma^2 + 4}}\right) \tag{A.10}$$

$$\Delta \varphi \to \frac{\pi}{2} + \sin^{-1}\left(\frac{\sigma}{\sqrt{\sigma^2 + 4}}\right) \tag{A.11}$$

Clearly, these are equal, and take the full range $0 < \Delta t = \Delta \varphi < \pi$ for $-\infty < \sigma < \infty$. Further, we can check that this family of geodesics indeed converge onto the boundary null geodesics. Figure 14 demonstrates these features. We see that as E increases, the geodesics accumulate at a finite value of Δt and $\Delta \varphi$, in this case σ being 1, $\frac{\pi}{2} + \sin^{-1}\left(\frac{1}{\sqrt{5}}\right) \approx \frac{\pi}{3}$.

To summarise this discussion, in pure AdS_{d+1} spacetime, null geodesics connect points on the boundary which are anti-podally located on the $\mathbf{S}^{d-1}$ at a time separation $\Delta t = \pi$. Spacelike bulk geodesics on the other hand connect points with $\Delta t = \Delta \varphi \neq \pi$ as illustrated by (A.10) and (A.11), respectively (or more generally, (A.2) and (A.3)).
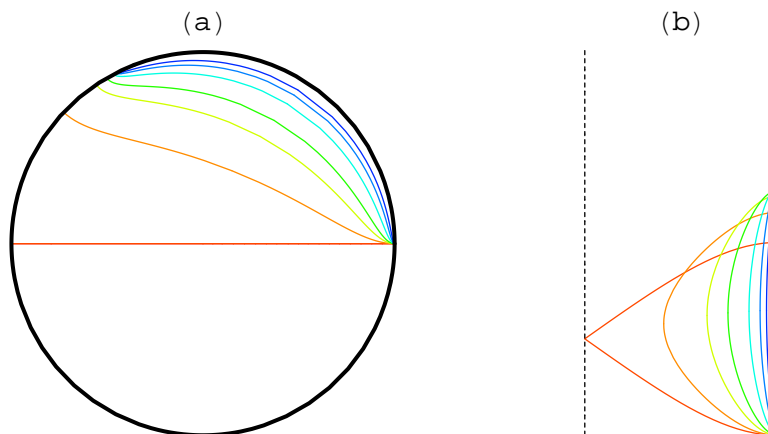
Figure 14: Spacelike geodesics in AdS, projected to **(a)** a constant t slice and **(b)** the $t-r$ plane, for increasing values of energy and $J^2 = E^2 - \sigma E$ with $\sigma = 1$ (in the infinite E limit this would yield $\Delta t = \Delta \varphi \approx \frac{\pi}{3}$). In **(a)** the boundary is indicated as the bold circle. In **(b)** the boundary at $\tan r = \frac{\pi}{2}$ is in bold and the dashed vertical line is the origin.

B. Radiation star in AdS

In this appendix, we construct the geometry corresponding to a gas of radiation in AdS and study its properties. As sketched out in section 3, constructing the solution entails specifying the form of the stress-energy-momentum tensor and solving the Einstein's equations.[26] After filling in the gaps in the presentation of section 3, we extend our study of the star geometry by analysing spacelike geodesics, and then discuss the observable differences between the star geometry and that of a black hole.

B.1 Construction of the star-AdS spacetime

As discussed in section 3, one can construct a simple model for a static, spherically symmetric, asymptotically AdS "star" geometry by solving Einstein's equations with a negative cosmological constant and matter given by a perfect fluid stress tensor corresponding to radiation. The metric coefficients are determined by solving the Einstein's equation

$$G_{ab} + \Lambda\, g_{ab} = 8\pi G_5\, T_{ab} \tag{B.1}$$

where for convenience we will set $8\pi G_5 \equiv 1$ and $\Lambda = -6$ to set AdS radius to unity.

The symmetries constrain the metric to take the form (3.2). One can then infer the equations (3.3) and (3.5) from the tt component of the Einstein tensor. The rr component of the Einstein tensor yields

$$\frac{f'}{f} = \frac{2}{r} \left(\frac{\frac{r^2}{R^2} + \frac{m(r)}{r^2} + \frac{1}{12}\,\rho(r)\,r^2}{\frac{r^2}{R^2} + 1 - \frac{m(r)}{r^2}} \right) \tag{B.2}$$

---

[26]Analogous calculations in 4 dimensions were discussed in [13], with similar qualitative results as we obtain below.
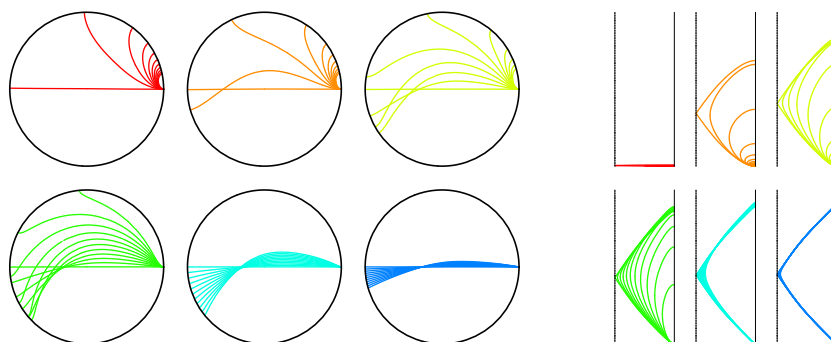
Figure 15: Spacelike geodesics in star with $\rho_0 = 10$ in AdS, projected to a constant t slice (left) and the $t - r$ plane (right), for six different values of energy ($E = 0, 2, 5, 10, 30, 80$). For each E, geodesics with different values of angular momentum ($J = 0, 1, 2, \ldots, 10$) are plotted. The bold circles represent the boundary at $\tan r = \frac{\pi}{2}$. The dashed vertical lines correspond to the origin $r = 0$ and the bold vertical lines to the boundary at $\tan r = \frac{\pi}{2}$. The range of t plotted is $(0, 1.1 \Delta t_0)$.

which can be easily integrated to get $f(r)$ in terms of $m(r)$ and $\rho(r)$. Finally, using the angular part of Einstein's equation, or equivalently the stress tensor conservation, we can write (for general equation of state)

$$\frac{dP}{dr} = -(\rho + P) \frac{1}{2} \frac{f'}{f} \tag{B.3}$$

This can then be used to derive the system of coupled first order ODEs for $m(r)$ and $\rho(r)$ given by (3.6) and (3.7), respectively. The equation for $f(r)$, (B.2), can be simplified to (3.4) using the equations for $m(r)$ and $\rho(r)$.

B.2 Geodesics in the star geometry

In section 3 we examined some aspects of the star geometry by focusing on null geodesics; here we extend this analysis to spacelike geodesics as well. While these do not lead to singularities of the boundary correlators, they nevertheless reveal interesting points. Since the star in AdS can be vied as a deformation of the pure AdS geometry, it is particularly interesting to contrast the behaviour of spacelike geodesics in the star geometry with that in AdS. In figure 15 we show spacelike geodesics projected onto the constant t and $t - r$ plane (these plots are to be compared with figure 13, where same conventions apply). As for null geodesics, we see a focusing effect, created by the star in the center of AdS.

To see how the endpoints of these various geodesics compare, let us consider the values Δt and $\Delta \varphi$ for the various geodesics. Figure 16 summarizes this. One interesting feature to note is that since the curves for various energies intersect each other, it is no longer true that for *any* two spacelike-separated points, there is a unique spacelike geodesic connecting them. In particular, unlike the pure AdS case, there is an open set of endpoints which can be reached by more than one geodesic. Even more remarkably, there exists a set of endpoints (lower branch of the thick pink curve in figure 16) which are connected by both a null and a spacelike geodesic! Also, as a corollary, it is no longer true that the
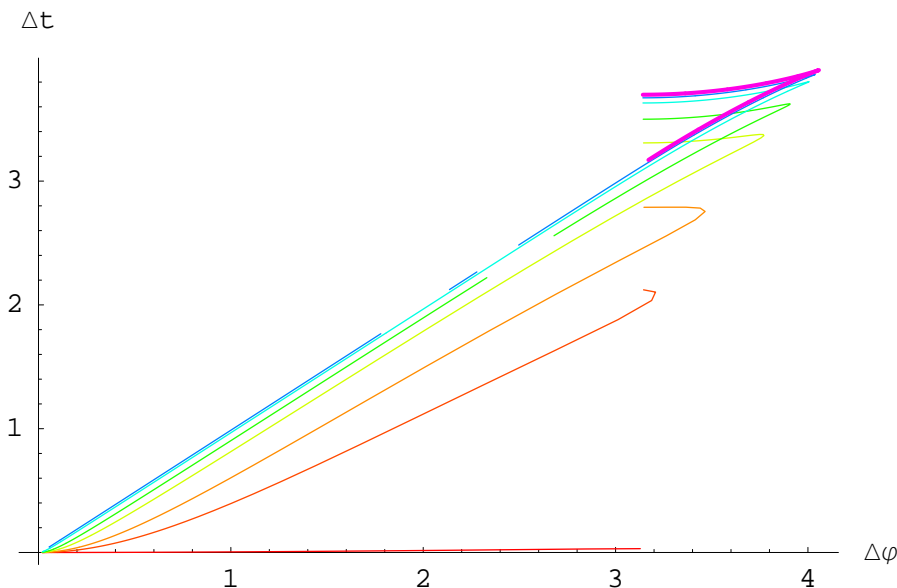
Figure 16: Endpoints of spacelike and null geodesics in the geometry of star with $\rho_0 = 10$ in AdS. Spacelike geodesics for six different values of energy ($E = 0, 2, 5, 10, 30, 80$) and a null geodesic (thick pink curve) is plotted for varying values of J – varying J traces out curves in the $\Delta t - \Delta\varphi$ plane; the top of the curves corresponds to small values of J, while in the large J limit, Δt and $\Delta\varphi$ both approach their starting value, namely 0.

endpoints of null geodesics lie on the boundary of the set of endpoints of spacelike geodesics. Correspondingly, the enpoints of the null geodesics reflect this behaviour, as can be seen easily in figure 5. While $\Delta\varphi$ slowly increases with increasing ρ_0, the endpoints never approach a straight line, as would be the case for the black hole geometry. This in turn means that the endpoints are less sensitive indicator of the star geometry than in the black hole case.

B.3 Comparison between star and black hole

Let us now ask how does the geometry vary with ρ_0. Clearly, as $\rho_0 \to 0$, the geometry becomes that of pure AdS; hence the star's utility in studying small perturbations on AdS. One might naively expect that in the opposite limit, as we make the internal density very large, the star should start behaving more and more like a black hole. Unfortunately, this is not the case, as will be explained below.

First of all, to compare the star's geometry with that of a Schwarzschild-AdS black hole, the most sensible map of parameters is to identify the black hole's mass with the star's total mass, so that the asymptotic geometry matches. In other words, for the black hole, we use the metric of the form in (3.2), but with

$$f(r) = h^{-1}(r) = \frac{r^2}{R^2} + 1 - \frac{M}{r^2} , \qquad \text{where} \quad M \equiv \lim_{r \to \infty} m(r) \qquad \text{(B.4)}$$

Now, consider the variation of the star's density and mass profiles as we increase ρ_0. This is plotted in figure 17. We see that as the star's total "extent" does not seem to change
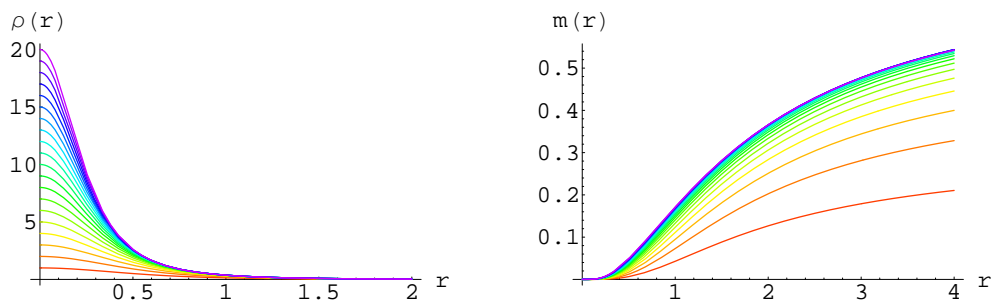
Figure 17: Density profile, and corresponding mass profile, for a star with various values of ρ_0 (which can be read off from values of $\rho(r = 0)$).
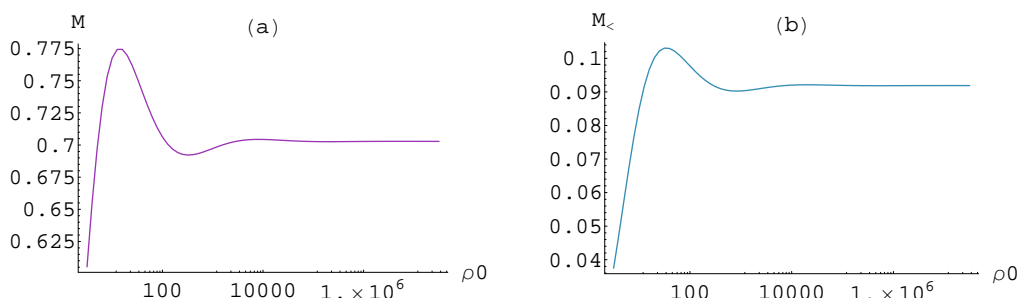

Figure 18: Star's total mass (a), and the fraction of the star's mass confined to within this radius, plotted as a function of ρ_0.

much with ρ_0 – the star is always confined within a size of order the AdS radius. This is of course due to the confining potential of the AdS geometry. Now, if the total mass could be made arbitrarily large, then for $M \gtrsim 1$, the star would be confined within its own Schwarzschild radius, and should be viewed as a black hole. However, we see that while the density can be increased, the mass is bounded from above, and becomes largely independent of ρ_0 after some point. This is illustrated more clearly in figure 18, where (a) the total mass, and (b) the fraction of the star's mass confined to within its effective Schwarzschild radius is plotted as a function of ρ_0. The left plot shows clearly that the total mass is bounded[27] from above by a rather small value: $M \leq 0.775R$. Curiously enough, the mass is not a monotonic function of the internal density.[28] In fact, when examined in more detail, $M(\rho_0)$ appears to exhibit certain self-similarity; however we will not detour into this intriguing observation further. We also find that the effective Schwarzschild radius (*i.e.*, what would be the Schwarzschild radius for a black hole with the total mass plotted

---

[27]In fact, this result is analogous to the similar result in the more familiar 4-dimensional, asymptotically flat static spherically symmetric spacetime, where given a fixed size R_* of a star (with any equation of state), the maximum possible mass such a star can attain is $M_{\max} = 4R_*/9$. [30]

[28]This might correspond to onset of some sort of radial instability, though there does not seem to be any obvious pathology. Correspondingly, we'll continue to include such high-ρ_0 solutions in our considerations. For the stars in 4-dimensional, asymptotically flat static spherically symmetric spacetime, [31] argued that an instability sets in at the turnover point where the mass function is non-monotone.
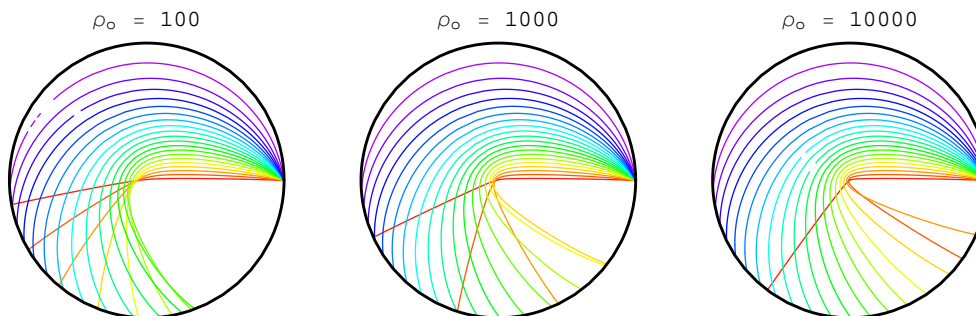
Figure 19: Null geodesics in AdS star with three different values of ρ_0 as indicated, projected onto a constant t slice, for varying angular momentum to energy ratio.

in figure 18a) is bounded by $r_+ \leq 0.716R$, so the star could at best be compared with a small Schwarzschild-AdS black hole. Most importantly, figure 18b shows that the mass contained within the effective Schwarzschild radius is a small fraction of the total mass (less than 11%), so that the star does *not* approach a black hole in any regime. In other words, we should not expect to obtain behaviour characteristic of a presence of an event horizon for any value of ρ_0.

   We have seen that the star made up of a gas of radiation can never develop an event horizon, so it cannot look like a black hole, no matter how high its internal density ρ_0. In section 3 we have further argued for the absence of null circular orbits, and emphasized that the corresponding geodesic endpoints demonstrate a clear difference between a star and a black hole. To illustrate this further, in figure 19 we plot the null geodesics, projected to a constant t slice, for increasing values of ρ_0. (This is the same plot as in the left plot in figure 4, which had $\rho_0 = 10$, redone for $\rho_0 = 100, 1000$, and 10000, as indicated.) We see that even at very large ρ_0, there is no null orbit. Even though the bending increases with ρ_0, it does so ever more slowly, rather analogously to the time delay for radial geodesics (*cf.* figure 3).

C. Eternal black hole in AdS

We now discuss some interesting properties of spacelike geodesics in the Schwarzschild-AdS background. The geodesic equations are given in (4.4). The quantity of interest for spacelike geodesics is $(\Delta t(E, J), \Delta\varphi(E, J))$ which depends on both E and J.

   The effective potential $V_{eff}(r)$ given in (4.5) for spacelike geodesics has two real zeros at $r = J$ and $r = r_+$, respectively. For $J < r_+$, $V_{eff}(r) < 0$ for $r > r_+$, so for any E, the spacelike geodesic will fall into the horizon[29] and will not come back to the same boundary. We are not interested in these geodesics. For $J > r_+$, $V_{eff}(r)$ has a maximum $V_c(J) = V_{eff}(r_m)$ at a value $r_m > r_+$ (see figure 20). For $E^2 > E^2_{max}(J) = V_c(J)$, the geodesic will again fall into the horizon. Thus for a spacelike geodesic to come back to the

---

[29]Subsequently it will either reach the other boundary or fall to the singularity.
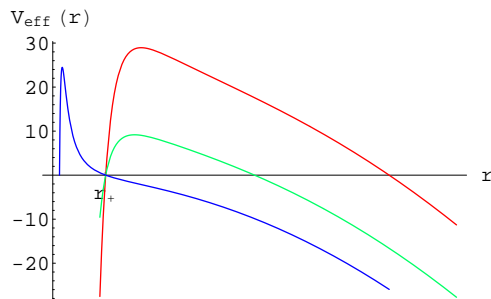
Figure 20: Plots of $V_{eff}(r)$ for $J = 5, 3, 0.1$, which correspond to red, green and blue curves respectively. The horizon is at $r_+ = .78$ (for $\mu = 1$). For $J < r_+$ (e.g. blue curve), geodesics will fall into the horizon and will not come back to the same boundary for any E. Similarly for $E > E_{max}$. E_{max} is the maximal value of V_{eff}.
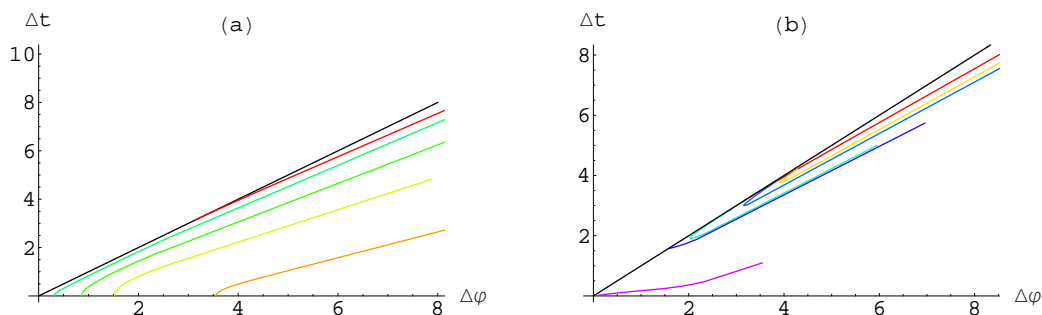

Figure 21: The end points of various spacelike geodesics in AdS BH (with $\mu = 1$ and $r_+ = 0.78$). Black and red line correspond to boundary and bulk null geodesics respectively as in figure 7. (a): Various curves show how end points change as E is varied from $E = 0$ to $E_{max}(J)$ with fixed J corresponding to $J = 0.8, 1.2, 2.2, 6.5$. The curve with larger J is farther away from the the lines corresponding to the null geodesics. Note that at $E = 0$, all lines start at real axis and as $E \to E_{max}(q)$, Δt and $\Delta \varphi$ go to infinity. (b): Various lines describe how end points change with J for a fixed $\alpha = E/J = 1.1$, 1.08, 1.02, 1, 0.2. The line with bigger value of α is closer to the lines of null geodesics. J varies from some finite J_c to ∞. It is clear that as $J \to \infty$ all curves approach their corresponding points on the null curve. Note that a curve with $0 < \alpha < 1$ will end up at the origin as $J \to \infty$. A curve with $\alpha = 1$ could end up anywhere in the diagonal line between the origin and (π, π) depending the value of $E - J$ which should be fixed in the limit $E, J \to \infty$.

same boundary, J and E should lie in the range $J \in (r_+, \infty)$ and $E \in (0, E_{max}(J))$ for a given J.

For a fixed $J > r_+$, at $E = 0$, $(\Delta \varphi(0, J), \Delta t(0, J)) = (\Delta \varphi_c(J), 0)$. $\Delta \varphi_c(J)$ is a monotonic function of J. As $J \to \infty$, $\Delta \varphi_c(J) \to \frac{2}{J} \to 0$, while as $J \to r_+$, $\Delta \varphi_c(J) \to \infty$ logarithmically. As E varies from 0 to $E_{max}(J)$, $\Delta t(E, J)$ and $\Delta \varphi(E, J)$ appear to monotonically increase to infinity (see figure 21). As $E \to E_{max}(J)$, it can be shown that

$$\Delta t(E, J) \approx \frac{1}{s(J)} \Delta \varphi(E, J) \to \infty \tag{C.1}$$

where $s(J)$ is given by

$$s(J) = \frac{J f(r_m)}{E_{max} r_m^2} = \sqrt{1 + \frac{\mu}{r_m^4(J)}} \qquad (C.2)$$

Recall that $r_m(J)$ is the maximum of $V_J(r)$. Note that $r_m(J = r_+) = r_+$ and as $J \to \infty$, $r_m(J) \to (2\mu)^{\frac{1}{2}}$. One can also check numerically that $r_m(J)$ is a monotonic function of J. From the second equality of (C.2), $s(J)$ is then a monotonic function of J decreasing from $s(J = r_+) = \sqrt{2 + \frac{1}{r_+^2}}$ to $s(J = \infty) = \alpha_0$, where α_0 was introduced in (4.6).

From the above discussion we conclude that the end points of spacelike geodesics cover the whole region bounded by the red curve corresponding to the bulk null geodesics, the straight line from the origin to (π, π), and the horizonal axis in figure 7. It is important to emphasize that φ is a periodic variable, so in various figures, the fundamental region is the strip $\varphi \in (-\pi, \pi]$. As a result we conclude that

1. For any end point $(\Delta\varphi, \Delta t)$ of a null geodesic (including boundary ones), there are an infinite number of spacelike geodesics ending at that point due to the periodicity of φ.

2. The bulk and boundary null geodesics can also share their end points for special values of Δt and $\Delta\varphi$.

Finally let us comment on how to obtain null geodesics from spacelike geodesics by taking a limit. It is easy to see that we see that the equations for spacelike geodesics approach those of null geodesics in the limit of $E, J \to \infty$ while keeping the ratio $\alpha = E/J$ fixed. More explicitly, the end point of a spacelike geodesic with $0 \le \alpha < 1$ will approach the origin in the $J \to \infty$ limit. A spacelike geodesic with $\alpha = 1$ will approach a boundary null geodesic in the limit. Its end point can be anywhere in the straight line between the origin and (π, π) depending the value of $E - J$ which should be fixed in the limit $E, J \to \infty$. A spacelike geodesic with $\alpha \in (1, \alpha_0)$ will approach a bulk null geodesic in the limit. A spacelike geodesic with $\alpha > \alpha_0$ will not come back to the same boundary. Figure 21 plots the end points of spacelike geodesics with E/J fixed.

D. No coming back for Poincaré patch

In the following we argue that for field theories formulated on $\mathbf{R}^{d-1,1}$ and states respecting the full Poincaré symmetry there are no new light-cone singularities. As discussed in section 2, the presence of light-cone singularities in the boundary field theory is governed by the properties of bulk null geodesics. For field theories formulated on $\mathbf{R}^{d-1,1}$ we will show that there are no null geodesics through the bulk spacetime connecting boundary points. This implies that the only null geodesics that connect points on the boundary are those that lie entirely within the boundary and hence the nature of singularities in the correlation function is entirely determined by the boundary causal structure.

To establish the absence of null geodesics connecting boundary points through the bulk, let us consider a bulk spacetime with negative cosmological constant foliated by

$\mathbf{R}^{d-1,1}$ slices. The metric can be written in the warped-product form by picking a metric $g_{mn}(x^i)$ on the boundary and a radial coordinate r:

$$ds^2 = e^{2A(r)} \, g_{mn} \, dx^m \, dx^n + dr^2 \tag{D.1}$$

For this geometry one can write down the geodesic equations as

$$\begin{aligned} \dot{r}^2 + e^{2A(r)} \, g_{mn} \, \dot{x}^m \dot{x}^n &= \kappa \ , \\ \ddot{r} - A'(r) \, e^{2A(r)} \, g_{mn} \, \dot{x}^m \dot{x}^n &= 0 \end{aligned} \tag{D.2}$$

with κ being $\pm, 0$ for spacelike, timelike and null geodesics, respectively. By eliminating the boundary directions we can write an effective classical particle in a potential equation for the motion in the radial direction:

$$\ddot{r} + A'(r) \, (\dot{r}^2 - \kappa) = 0 \tag{D.3}$$

The issue of whether geodesics emanating from the boundary into the bulk turn around, can now be analyzed simply in the effective problem for the radial motion (D.3). For the case of null geodesics which we are especially interested in the first integral from (D.2) gives:

$$\dot{r} = \frac{C}{e^{A(r)}} \tag{D.4}$$

implying that $A(r) \to \infty$ for the geodesic to turn around (since $\dot{r} = 0$ by definition at the turn around point).

However, $A(r)$ cannot diverge to ∞ – the energy condition on the stress tensor require that $A'(r)$ be a monotonically decreasing function [32]. This effectively implies that $A(r)$ decreases from ∞ at the AdS boundary where the field theory is formulated. Physically divergence of $A(r)$ would look like we have second timelike boundary in the geometry which again is disallowed by the null geodesic convergence condition in spacetimes where the matter sources respect the null energy condition.

Note that this result is contingent on the Poincaré symmetries of the boundary being preserved.[30] We can have geodesics that return to the boundary even in the non-compact case when we consider states that break the boundary Poincaré invariance. A simple example is to consider the global AdS-Schwarzschild geometry that is sliced in the Poincaré coordinates (*cf.*, [1] for a boundary description of this state). Here it is possible to exploit the black hole, which breaks the Poincaré symmetry to slingshot oneself back to the boundary in a timescale shorter than the AdS time.

E. Collapsing shell in AdS

In section 5 we derived a scaling formula for t_o as a function of $\delta t = t_h - t_i$ using a ray tracing calculation. The exponential relation is given in (5.6) and intuitively we can imagine this arising from the red-shift in the vicinity of the horizon. We now proceed to derive this

---

[30]We thank Simon Ross for pointing this out to us and suggesting the example described.

result more explicitly, by finding actual radial null geodesics in the collapse background. In this appendix we constrain ourselves to the sharp shell cleanly separating AdS and Schwarzschild-AdS; in appendix F we consider the more general smeared shell collapse modeled by a Vaidya spacetime and also extend our analysis to non-radial geodesics.

Consider the set-up as sketched in figure 8. There are two interesting limits to consider as discussed in section 5.3. In particular, we wish to obtain the leading behaviour both as $t_i \to t_h^{\pm}$ and as $t_i \to t_s$, as indicated in figure 12a and b, respectively. In fact, in order to derive both (5.6) and the scaling exponent γ introduced in section 5.3, we will find the full exact expression for t_o in terms of t_i and the parameters t_s and r_+ describing the shell. It is interesting to examine the geodesic behavior both in $d = 3$ and in $d = 5$. The distinction of course is engendered by the fact that the BTZ black hole in $d = 3$ being an orbifold of AdS_3 is a simpler geometry. On the other hand, the physics of the type III geodesics of figure 8b is different is quite different since spacelike geodesics do not bounce off the BTZ singularity, so we can meaningfully consider only the $t_i \to t_h^-$ scaling.

The strategy for calculating radial null geodesics will be to write the geodesics in the different coordinate patches (such that in each patch we can use the metric of the form in (5.1)), and then patch them together using the fact that both the geodesics and the shell are null. The three regions of interest are depicted in figure 12c, and correspond to

1. pure AdS (before/inside the shell)

2. Schwarzschild-AdS, outside the horizon (outside the shell)

3. Schwarzschild-AdS, inside the horizon (but still outside the shell)

E.1 $d = 3$

As a warm-up, let us first focus on $d = 3$. For simplicity, we use the metric (5.1) with $f(r) = r^2 + 1$ in region 1, and $f(r) = r^2 - r_+^2$ in regions 2 and 3. We will write the expressions for geodesics in 3 distinct regions (even though in 3 dimensions, region 3 is not so relevant since radial spacelike geodesics in BTZ do not bounce off the singularity). Calculating the geodesics as before, we have for pure AdS:

$$t_{AdS}(r) = t_0 \pm \left(\tan^{-1} r - \tan^{-1} r_0 \right) \tag{E.1}$$

and for BTZ:

$$
\begin{aligned}
t_{BTZ}(r) &= t_0 \mp \frac{1}{r_+} \left(\tanh^{-1} \frac{r}{r_+} - \tanh^{-1} \frac{r_0}{r_+} \right) \qquad \text{inside} \\
&= t_0 \pm \frac{1}{2r_+} \ln \left[\left(\frac{r - r_+}{r + r_+} \right) \left(\frac{r_0 + r_+}{r_0 - r_+} \right) \right] \qquad \text{outside}
\end{aligned} \tag{E.2}
$$

where we denote the initial conditions by $t(r_0) \equiv t_0$. We can now patch these together to see when a geodesic starting at $t = t_i, r = \infty$ reemmerges back out to $r = \infty$. Denoting this time t_o, we can express t_o in terms of t_i, t_s, and r_+, obtaining:

$$t_o = t_s + \frac{1}{r_+} \ln \left(\frac{\tan(\frac{t_s - t_i}{2}) + r_+}{\tan(\frac{t_s - t_i}{2}) - r_+} \right) \qquad \text{if } t_o < t_h \tag{E.3}$$

Matching where the shell intersects the horizon, we can relate t_s to t_h as follows:

$$t_s = t_h + 2 \tan^{-1} r_+ \tag{E.4}$$

Finally, substituting (E.4) into (E.3) and expanding for small δt, we obtain the scaling behaviour

$$t_o \sim -\frac{1}{r_+} \ln |\delta t| \quad \Longrightarrow \quad \delta t \sim -e^{-r_+ t_o} = -e^{-\kappa t_o} \qquad \text{as } t_o \to \infty \tag{E.5}$$

where $\kappa = r_+$ is the surface gravity of the BTZ black hole.

Unfortunately, in this set-up we can only answer the first part of the questions raised in section 5.3: as $\delta t \to 0^-$, t_o diverges logarithmically with the coefficient given by the black hole temperature, as one would naively expect. To see the other scalings, $t_i \to t_h^+$ and $t_i \to t_s$, discussed in section 5.3 , we need to go to higher dimensions.[31]

E.2 $d = 5$

Now let us consider $d = 5$. Whereas the time-radius relation for radial geodesics is independent of the dimension in pure AdS, we have a more complicated relation $t(r)$ for the black hole geometry than in the BTZ case. Writing

$$t(r) = t(r_0) \pm \int_{r_o}^{r} \frac{d\bar{r}}{f(\bar{r})} \tag{E.6}$$

and rewriting the metric function outside the shell as

$$f(r) = \frac{(r^2 + \rho_+^2)(r^2 - r_+^2)}{r^2} \tag{E.7}$$

where $\rho_+^2 \equiv 1 + r_+^2$, we can express the indefinite integral pertaining to outside and inside horizon regions respectively as

$$\int \frac{dr}{f(r)} = \frac{1}{r_+ \kappa} \left(\rho_+ \tan^{-1} \frac{r}{\rho_+} - r_+ \tanh^{-1} \frac{r_+}{r} \right) \qquad \text{for } r > r_+ \tag{E.8}$$

$$\int \frac{dr}{f(r)} = \frac{1}{r_+ \kappa} \left(\rho_+ \tan^{-1} \frac{r}{\rho_+} - r_+ \tanh^{-1} \frac{r}{r_+} \right) \qquad \text{for } r < r_+ \tag{E.9}$$

where $\kappa = \frac{1 + 2r_+^2}{r_+}$ is the surface gravity of the black hole. For a geodesic crossing the horizon, the infinite contribution from the coordinate singularity cancels out, so if $r_1 > r_+$ and $r_2 < r_+$, say, we would obtain

$$t_{SAdS}(r_2) = t_{SAdS}(r_1) - \frac{1}{r_+ \kappa} \left(\rho_+ \tan^{-1} \frac{r}{\rho_+} \Big|_{r_1}^{r_2} + r_+ \tanh^{-1} \frac{r_+}{r_1} - r_+ \tanh^{-1} \frac{r_2}{r_+} \right) \tag{E.10}$$

---

[31]If we nevertheless ignore the fact that spacelike geodesics do not bounce off the singularity, and consider the two null geodesics meeting at the singularity, then we would expect to find 1) the same scaling behaviour (same coefficient) as in (E.5) for $t_i > t_h$, and 2) $(t_s - t_i) \sim (t_o - t_s)$ (i.e. $\gamma = 1$).

Applying this to the geodesics of type II and III in figure 12a, we obtain the full exact expression for t_o in terms of t_s, the parameters specifying the black hole, and the radius of where the shell crosses our geodesic r_c:

$$t_o = t_s + \frac{2}{r_+ \kappa} \left(\rho_+ \frac{\pi}{2} - \rho_+ \tan^{-1} \frac{r_c}{\rho_+} + r_+ \tanh^{-1} \frac{r_c}{r_+} \right) \qquad \text{for geod. } II \qquad \text{(E.11)}$$

$$t_o = t_s + \frac{2}{r_+ \kappa} \left(-\rho_+ \tan^{-1} \frac{r_c}{\rho_+} + r_+ \tanh^{-1} \frac{r_c}{r_+} \right) \qquad \text{for geod. } III \qquad \text{(E.12)}$$

where (in both cases) the crossing radius is given by

$$r_c = \tan \left(\frac{t_s - t_i}{2} \right) \qquad \text{(E.13)}$$

and the time of the shell is related to the time of horizon formation by

$$t_s = t_h + 2 \tan^{-1} r_+ \qquad \text{(E.14)}$$

We can easily expand this out for small δt, to check that in both cases

$$|\delta t| \approx e^{-\kappa t_o} \qquad \Longrightarrow \qquad t_o \sim \frac{1}{\kappa} \ln \frac{1}{|\delta t|} \ . \qquad \text{(E.15)}$$

This is again consistent with our expectations (5.6), and indeed of the same form as the result obtained for the 3-dimensional case.

Finally, we can also use expression (E.12) to consider the case of figure 12b. In particular, if we let $t_s - t_i \equiv \varepsilon$, then expanding $t_o - t_s$ to third order in ε, we find that

$$t_o - t_s \approx \frac{1}{12 \, r_+^2 \, \rho_+^2} \varepsilon^3 \ . \qquad \text{(E.16)}$$

This in particular implies that the scaling parameter γ introduced in section 5.3 is 3 for black hole formation in $d = 5$. Intriguingly, we can generalize this to d dimensions: For d-dimensional collapse spacetime, $\gamma = d - 2$.

F. Smeared shell in AdS and non-radial geodesics

In appendix E, we have considered radial null geodesics in the collapsing null shell geometry. In particular, we calculated t_o as a function of t_i and the shell parameters. As discussed in section 5, being able to read off the value of t_i for which t_o diverges from the gauge theory correlators, we can automatically determine the horizon formation time t_h ($\Longrightarrow t_H$). Here we wish to extend this analysis in two directions. First, we want to consider a more general (and physically more realistic) background corresponding to a smeared shell. Second, we want to analyze non-radial geodesics, as motivated in section 5. To that end, we will discuss general null geodesics in Vaidya-AdS spacetime.

F.1 Vaidya for AdS

Consider the stress tensor for a spherical null gas

$$T_{vv} = h(r, v) \tag{F.1}$$

The metric can be written as

$$ds^2 = -f(r, v)\, dv^2 + 2\, dv\, dr + r^2\, d\Omega_3^2 \tag{F.2}$$

with

$$f(r, v) = r^2 + 1 - \frac{m(v)}{r^2} \tag{F.3}$$

The covariant conservation $\nabla^\mu T_{\mu\nu} = 0$ of T implies that[32]

$$h(r, v) = \frac{1}{r^3} q(v) \tag{F.4}$$

The Einstein equations now reduce to (with $\Lambda = -6$)

$$m'(v) = \frac{2}{3} q(v) \tag{F.5}$$

For the sharp shell we take $q(v)$ has the form of a delta function, *i.e.*,

$$m(v) = 0 \qquad v < v_0 \tag{F.6}$$
$$= \mu \qquad v > v_0 \tag{F.7}$$

with $q(v) = \frac{3}{2}\mu\, \delta(v - v_0)$. Note that in this case the v-dependence disappears before and after the shell; the spacetime (F.2) is static in both regions (but not globally static because of the shell), written in ingoing coordinates,

$$v = t + z, \qquad dz = \frac{dr}{f} \tag{F.8}$$

F.2 Null geodesics

Let us now consider null geodesics in the background (F.2). Writing the second-order geodesic equation (in the equatorial plane) directly yields

$$\ddot{v} + \tfrac{1}{2}\, \partial_r f(r, v)\, \dot{v}^2 - r\, \dot{\varphi}^2 = 0$$
$$\ddot{r} - \tfrac{1}{2}\left[\partial_v f(r, v) + f(r, v)\, \partial_r f(r, v)\right] \dot{v}^2 - r\, f(r, v)\, \dot{\varphi}^2 = 0$$
$$\ddot{\varphi} + \tfrac{2}{r}\, \dot{r}\, \dot{\varphi} = 0 \tag{F.9}$$

For any given $f(r, v)$, we can solve these numerically to find any geodesic through the bulk. The function $f(r, v)$ with which we choose to model the smeared shell in section 5 is

$$f(r, v) = r^2 + 1 - \frac{\mu}{r^2}\left(\frac{1 + \tanh\frac{v}{v_s}}{2}\right) \tag{F.10}$$

---

[32]Note that $\Gamma_{rv}^v = \Gamma_{rr}^r = 0$.

which smoothly interpolates between AdS at $v \to -\infty$ and Schwarzschild-AdS as $v \to +\infty$. In particular, the shell is inserted at[33] $v = 0 = t_s + \pi/2$, and has 'thickness' v_s. This provides a convenient regulator of the thin shell collapse, since as $v_s \to 0$, we recover the collapse spacetime (5.1) written in ingoing coordinates.

However, to find the geodesics in the collapse spacetime, and specifically to determine $t_h(\alpha)$, we can use a simpler and more elegant method, which we now indicate. The geodesics can be obtained from the following action

$$S = \int d\tau \left(-\frac{1}{2} f \dot{v}^2 + \dot{v} \dot{r} + \frac{1}{2} r^2 \dot{\varphi}^2 \right) \tag{F.11}$$

The canonical momenta are

$$J = r^2 \dot{\phi}, \qquad E = -\frac{\partial L}{\partial \dot{v}} = -\dot{r} + f \dot{v}, \qquad \frac{\partial L}{\partial \dot{r}} = \dot{v} \tag{F.12}$$

Note that J is conserved, while E is in general not. Note that J can be scaled to be 1 by a rescaling of τ. As before, we will denote $\alpha = \frac{E}{J}$ and set $J = 1$. Another first integral of the system is given by

$$\dot{r}^2 + \frac{f}{r^2} = \alpha^2 \tag{F.13}$$

The equations of motion can now be written as

$$\dot{\alpha} = \frac{1}{2} \frac{\partial f}{\partial v} \dot{v}^2 \tag{F.14}$$

$$\ddot{v} = -\frac{1}{2} \frac{\partial f}{\partial r} \dot{v}^2 + \frac{1}{r^3} \tag{F.15}$$

From the above equations we can also derive

$$\ddot{r} = \frac{1}{2} \frac{\partial f}{\partial v} \dot{v}^2 - \frac{1}{2r^2} \frac{\partial f}{\partial r} + \frac{f}{r^3} \tag{F.16}$$

where we have used that

$$\dot{v} = \frac{\alpha + \dot{r}}{f} \tag{F.17}$$

Now we apply the above equations to the Vaidya spacetime with a sharp shell, in which case

$$\frac{\partial f}{\partial v} = -\frac{\mu}{r^{d-3}} \delta(v - v_0) \tag{F.18}$$

The discontinuity of f across $v = v_0$ is thus given by $\delta f = -\frac{\mu}{r^{d-3}}$. One can readily conclude from the above equations that both α and $\dot{r}$ jump across $v = v_0$, in fact by the same amount, while $\dot{v}$ is continuous. More explicitly we find that

$$\delta \dot{r} = \delta \alpha = -\frac{\mu}{2r^{d-3}} \dot{v} \Big|_{v_0} < 0 \tag{F.19}$$

Let us now return to the problem of determining $t_h(\alpha)$ for the collapse geometry. Realizing that α jumps across the shell, let us work backwards by considering what feature

<hr />

[33]Since both AdS and Schwarzschild-AdS geometries are static, we can WLOG set the time t_s of the shell's creation on the boundary; for convenience we choose $t_s = -\pi/2$.

of the geodesics makes t_o large. The relevant spacetime to consider is Schwarzschild-AdS, wherein the geodesics follow from the potential (4.5) drawn in figure 6. Since the top of the potential is always outside the horizon (as follows from the discussion in section 4, $r_m^2 = 2\mu = 2r_+^2 \left(r_+^2 + 1 \right) > r_+^2$), the only way that a non-radial null geodesic could emerge at infinite time would be to get trapped in the unstable circular orbit at the top of the effective potential. This requires

$$\alpha_o^2 = V_{eff}(r_m) = 1 + \frac{1}{4\mu} \tag{F.20}$$

Knowing the α in the Schwarzschild-AdS part of the spacetime, we can now use the expression (F.19) for the jump in α across the shell, to find what initial conditions (*i.e.* what α_i in AdS) we need to start with to achieve this α_o. Using (F.17), (F.13), and the expression for $f(r)$ in AdS (5.2), all evaluated at some crossing radius r_x where the geodesic intersects the shell, we can reexpress (F.19) as follows:

$$\alpha_o = \alpha_i - \frac{\mu}{2r_x^2} \frac{\alpha_i + \sqrt{\alpha_i^2 - \frac{r_x^2+1}{r_x}}}{r_x^2 + 1} \tag{F.21}$$

Finally, we can express the crossing radius r_x in terms of the initial time t_i by following the geodesic with parameter α_i from r_x back to its starting point on the boundary at t_i. This is given by

$$t_s - t_i = \tan^{-1} r_x + \tan^{-1} \frac{\sqrt{(\alpha_i^2 - 1)\, r_x^2 - 1}}{\alpha_i} \tag{F.22}$$

Note that t_i should be viewed as a function of α_i, and for $t_o \to \infty$, this is nothing but $t_h(\alpha)$ of section 5, where we have been using $\alpha \equiv \alpha_i$.

Hence, to find $t_h(\alpha)$, we can solve the system of equations (F.20), (F.21), and (F.22). We first solve (F.20) and (F.21) for the crossing radius $r_x(\alpha_i)$, and then substitute this into (F.22) to find $t_h(\alpha) = t_i$, as a function of $\alpha_i \equiv \alpha$ and the shell parameters, μ and t_s. This determines the black curve plotted in figure 9. Note that the radial geodesic limit ($\alpha \to \infty$) is continuous, despite the fact that only the radial geodesic can truly sample the horizon formation event, since only the null outgoing radial geodesics can escape from the close vicinity of the horizon.

References

[1] G.T. Horowitz and N. Itzhaki, *Black holes, shock waves and causality in the AdS/CFT correspondence*, *JHEP* **02** (1999) 010 [hep-th/9901012].

[2] D. Kabat and G. Lifschytz, *Gauge theory origins of supergravity causal structure*, *JHEP* **05** (1999) 005 [hep-th/9902073].

[3] S. Gao and R.M. Wald, *Theorems on gravitational time delay and related issues*, *Class. and Quant. Grav.* **17** (2000) 4999 [gr-qc/0007021].

[4] V.E. Hubeny, M. Rangamani and S.F. Ross, *Causal structures and holography*, *JHEP* **07** (2005) 037 [hep-th/0504034].

[5] J.P. Gregory and S.F. Ross, *Looking for event horizons using UV/IR relations*, *Phys. Rev.* **D 63** (2001) 104023 [hep-th/0012135].

[6] L. Fidkowski, V. Hubeny, M. Kleban and S. Shenker, *The black hole singularity in AdS/CFT*, *JHEP* **02** (2004) 014 [hep-th/0306170].

[7] G. Festuccia and H. Liu, *Excursions beyond the horizon: black hole singularities in Yang-Mills theories, I*, *JHEP* **04** (2006) 044 [hep-th/0506202].

[8] J. Louko, D. Marolf and S.F. Ross, *On geodesic propagators and black hole holography*, *Phys. Rev.* **D 62** (2000) 044041 [hep-th/0002111].

[9] P. Kraus, H. Ooguri and S. Shenker, *Inside the horizon with AdS/CFT*, *Phys. Rev.* **D 67** (2003) 124022 [hep-th/0212277].

[10] B. Freivogel et al., *Inflation in AdS/CFT*, *JHEP* **03** (2006) 007 [hep-th/0510046].

[11] J. Hammersley, *Extracting the bulk metric from boundary information in asymptotically AdS spacetimes*, hep-th/0609202.

[12] M. Kleban, J. McGreevy and S.D. Thomas, *Implications of bulk causality for holography in AdS*, *JHEP* **03** (2004) 006 [hep-th/0112229].

[13] D.N. Page and K.C. Phillips, *Selfgravitating radiation in anti-de Sitter space*, *GRG*, 1985.

[14] D. Astefanesei and E. Radu, *Boson stars with negative cosmological constant*, *Nucl. Phys.* **B 665** (2003) 594 [gr-qc/0309131].

[15] D. Astefanesei and E. Radu, *Rotating boson stars in (2+1) dimensions*, *Phys. Lett.* **B 587** (2004) 7 [gr-qc/0310135].

[16] G.T. Horowitz and V.E. Hubeny, *CFT description of small objects in AdS*, *JHEP* **10** (2000) 027 [hep-th/0009051].

[17] H. Lin, O. Lunin and J.M. Maldacena, *Bubbling AdS space and 1/2 BPS geometries*, *JHEP* **10** (2004) 025 [hep-th/0409174].

[18] S.D. Mathur, *The fuzzball proposal for black holes: an elementary review*, *Fortschr. Phys.* **53** (2005) 793 [hep-th/0502050].

[19] S.D. Mathur, *The quantum structure of black holes*, *Class. and Quant. Grav.* **23** (2006) R115 [hep-th/0510180].

[20] U.H. Danielsson, E. Keski-Vakkuri and M. Kruczenski, *Spherically collapsing matter in AdS, holography and shellons*, *Nucl. Phys.* **B 563** (1999) 279 [hep-th/9905227].

[21] S.B. Giddings and S.F. Ross, *D3-brane shells to black branes on the coulomb branch*, *Phys. Rev.* **D 61** (2000) 024036 [hep-th/9907204].

[22] S.B. Giddings and A. Nudelman, *Gravitational collapse and its boundary description in AdS*, *JHEP* **02** (2002) 003 [hep-th/0112099].

[23] K. Maeda, M. Natsuume and T. Okamura, *Extracting information behind the veil of horizon*, *Phys. Rev.* **D 74** (2006) 046010 [hep-th/0605224].

[24] S.W. Hawking, *Particle creation by black holes*, *Commun. Math. Phys.* **43** (1975) 199.

[25] V. Balasubramanian, V. Jejjala and J. Simon, *The library of babel*, *Int. J. Mod. Phys.* **D14** (2005) 2181–2186 [hep-th/0505123].

[26] V. Balasubramanian, J. de Boer, V. Jejjala and J. Simon, *The library of babel: on the origin of gravitational thermodynamics*, *JHEP* **12** (2005) 006 [hep-th/0508023].

[27] V. Balasubramanian, P. Kraus and M. Shigemori, *Massless black holes and black rings as effective geometries of the D1-D5 system*, *Class. and Quant. Grav.* **22** (2005) 4803 [hep-th/0508110].

[28] V. Balasubramanian, B. Czech, K. Larjo and J. Simon, *Integrability vs. information loss: a simple example*, *JHEP* **11** (2006) 001 [hep-th/0602263].

[29] M.W. Choptuik, *Universality and scaling in gravitational collapse of a massless scalar field*, *Phys. Rev. Lett.* **70** (1993) 9.

[30] R.M. Wald, *General relativity*, Chicago Univ. Pr., U.S.A., 1984, p. 491.

[31] R. Sorkin, *A criterion for the onset of instability at a turning point*, *Astrophys. J.* **249** (1981) 254.

[32] D.Z. Freedman, S.S. Gubser, K. Pilch and N.P. Warner, *Renormalization group flows from holography supersymmetry and a C-theorem*, *Adv. Theor. Math. Phys.* **3** (1999) 363 [hep-th/9904017].